Mineralium Deposita (2020) 55:1127–1147
https://doi.org/10.1007/s00126-019-00923-2

ARTICLE

The polyphase evolution of a late Variscan W/Au deposit (Salau, French Pyrenees): insights from REE and U/Pb LA-ICP-MS analyses

Thomas Poitrenaud[1,2] · Marc Poujol[3] · Romain Augier[1] · Eric Marcoux[1]

Received: 14 March 2018 / Accepted: 14 August 2019 / Published online: 3 September 2019

Abstract

The Salau deposit, located in the Axial Zone of the French Pyrenees, is the most important tungsten deposit ever mined in France. Two types of mineralization, both closely associated with a granodiorite intrusion, are distinguished. The first is a fine-grained scheelite skarn related to contact metamorphic and metasomatism between the intrusion and the adjacent carbonate rocks. The second type is represented by massive sulfides accompanied by coarse-grained scheelite, apatite, and electrum. This syn-kinematic mineralization is found enclosed within the skarn ore but occurs also within the granodiorite stock along major ductile–brittle shear zones. REE contents of scheelite and apatite from the two types of mineralization show differences suggesting that the two types derived from two different fluids. U/Pb dating on zircon, apatite and scheelite illustrates that magmatic zircon and apatite formed at 295 ± 2 Ma during emplacement and cooling of the granodiorite intrusion. These are cogenetic to the fine-grained scheelite skarn. Hydrothermal apatite from massive sulfide ores yields a younger age of 289 ± 2 Ma, whereas closely associated coarse-grained scheelite yields a consistent although less precise age of 284 ± 11 Ma. These results suggest that the late massive sulfide ore with abundant coarse-grained scheelite and electrum is related to the emplacement of an underlying, more evolved intrusion, accompanied during its ascent by the development of steeply dipping reverse-dextral shear zones.

Keywords Tungsten · Salau deposit · Polyphase ore formation · REE analyses · Scheelite U/Pb geochronology

Introduction

Mineral deposits are the result of a complex combination of geological processes that cause local metal enrichment in the Earth's crust. Geochemical tools may be applied to identify these processes. Among these tools, development of laser ablation inductively coupled plasma mass spectrometry (LA-ICP-MS) in situ analyses can provide either the age of the U-Th bearing phases associated with mineralization or their geochemical signature (Sylvester and Ghaderi 1997; Jackson et al. 2004; Cocherie et al. 2005; Harley et al. 2007; Raju et al. 2015; Mao et al. 2016; Poulin et al. 2018). Due to recent developments of U/Pb dating of minerals, geochronology now allows to date successive mineralizing and alteration events. A wide range of minerals and isotopic systems are now used for direct dating of ore minerals including Rb/Sr on sphalerite (Nakai et al. 1993; Christensen et al. 1995); Re/Os on sulfide minerals (Stein et al. 1998, 2000; Morelli et al. 2005); K/Ar and Ar/Ar on Mn oxides (Vasconcelos et al. 1992; Ruffet et al. 1996; Spier et al. 2006), illite (Bechtel et al. 1996; Clauer et al. 2015; Bozkaya et al. 2016), adularia (Lang et al. 1994; Sanematsu et al. 2006; Oze et al. 2017), lepidolite (Smith et al. 2005); or Sm/Nd on fluorite (Chesley et al. 1991, 1994), and scheelite (Bell et al. 1989; Anglin et al. 1996; Eichhorn et al. 1999). The U–Th/Pb system allows to date uraninite (Ludwig et al. 1987; Bowles 1990; Fayek et al. 2002; Ballouard et al. 2017, 2018), heterogenite (Decrée et al. 2010, 2014), apatite (Pochon et al. 2016; Ballouard et al. 2018), columbite–tantalite (Romer and Wright 1992; Romer and Lehmann 1995; Smith

Editorial handling: J. Gutzmer

Electronic supplementary material The online version of this article (https://doi.org/10.1007/s00126-019-00923-2) contains supplementary material, which is available to authorized users.

✉ Thomas Poitrenaud
thomas.poitrenaud@hotmail.fr

[1] Institut des Sciences de la Terre d'Orléans, UMR 7327 – CNRS / Université d'Orléans /BRGM, 1A rue de la Férollerie, 45071 Orleans Cedex 2, France

[2] Present address: Mines du Salat, 8 Esplanade Compans Caffarelli, 31000 Toulouse, France

[3] Géosciences Rennes, UMR 6118 – Univ Rennes/CNRS, 35000 Rennes, France

et al. 2004; Che et al. 2015; Melleton et al. 2015; Fosso Tchunte et al. 2018), wolframite (Frei et al. 1998; Romer and Lüders 2006; Harlaux et al. 2018), cassiterite (Gulson and Jones 1992; Yuan et al. 2008), and scheelite (Wintzer et al. 2016) or bastnaesite (Ntiharirizwa et al. 2018).

The Axial Zone of the Pyrenees (France) comprises Paleozoic rocks affected by polyphased tectonometamorphic events during the Variscan and Alpine events (Casas et al. 1989; Vissers and Meijer 2012; Denèle et al. 2014; Cochelin et al. 2017). The area is known to host several tungsten and gold deposits and occurrences (Derré 1973; Guy 1988). Among these, the Salau deposit was the most important tungsten mine in France, with a production of 13,950 t WO_3 between 1970 and 1986, with an exceptional high average grade of 1.5% WO_3. The deposit is located at the contact between the la Fourque granodioritic intrusion and metacarbonate host rocks. The ore, traditionally considered as a scheelite skarn, has a complex mineralogy and morphology, affected by a late "hydrothermal alteration" (Fonteilles et al. 1989). Similar skarn occurrences exist in the vicinity of Salau, such as Aurenere, in Spain (Fig. 1).

In addition to scheelite, the Salau deposit also contains gold in economic concentrations (1–10 g/t; Guiraudie et al. 1963; Fonteilles et al. 1989). However, the ore-forming processes and the paragenetic position of gold remain unclear. Some authors considered that sulfides, related to the late "hydrothermal alteration," are the retrograde stage of the scheelite skarn formation (Fonteilles et al. 1988). Other studies interpreted these sulfides as the expression of a shear zone mineralization without a genetic link with the La Fourque intrusion (Ledru and Autran 1987). This results, in part, from the fact that neither the emplacement age of the intrusive rocks nor metal deposition has been dated. The age of intrusion and skarn is interpreted to be late Variscan (Derré 1973). Similarly, deformation along the shear zone is the latest deformation event in the deposit (Kaelin 1982).

The aim of this paper is to constrain the timing and the origin of high-grade W/Au mineralization during the late-orogenic evolution of the Axial Zone of the Pyrenees. The Salau deposit and Aurenere occurrence were studied in order to characterize mineralization using field, petrography, SEM imagery, whole rock, and mineral geochemistry (apatite, scheelite). In addition, LA-ICP-MS U/Pb in situ dating on zircon, apatite, and scheelite was performed to constrain ages of emplacement of the intrusive rocks or of mineralizing event(s).

Geological background

Regional geology

The Pyrenees are an east–west trending Alpine orogenic segment located between France and Spain. The Axial Zone of the Pyrenees is a segment of the southern external zone of the Variscan belt, which has structured the whole western Europe at the end of the Paleozoic, mostly during the Pennsylvanian (Garcia-Sansegundo et al. 2011). Ediacarian to Paleozoic metasedimentary and plutonic rocks related to the Variscan orogeny crop out in the Axial Zone (Fig. 1). A strong structural contrast exists in the Axial Zone between middle crust rocks with flat-lying foliation and the upper crust rocks with a steeply dipping schistosity (Carreras and Capellà 1994; Denèle et al. 2009a; Cochelin et al. 2017). Four major successive deformation events have been documented (Denèle et al. 2009a; Laumonier et al. 2010; Denèle et al. 2014; Cochelin et al. 2017). The first stage is of crustal thickening during N–S to NE–SW compressive tectonics, responsible for fold–thrust belt development in the upper crust (323–310 Ma; Bodin and Ledru 1986). The second stage is localized in the middle crust (310–305 Ma). This is a crustal-scale stage of syn-convergence and horizontal lateral flow of the middle crust contemporaneous with the HT/LP metamorphic peak and partial melting (Vilà et al. 2007). The third stage corresponds to deformation in reverse-dextral shear zones during cooling of the Variscan crust as exemplified by the Merens shear zone (Denèle et al. 2008). The activity of the shear zone has never been dated using robust methods. The latest stages of deformation are marked by a strong heat anomaly at the bottom of the upper crust between ca. 305 to 285 Ma (Romer and Soler 1995; Aguilar et al. 2014). The emplacement of calc-alkaline and more evolved plutons is responsible for contact metamorphism, locally accompanied by skarn formation (Autran et al. 1970; Fonteilles et al. 1989; Soler et al. 1990; Cardellach et al. 1992; Ayora and Casas 1995; Barnolas and Chiron 1996). Several scheelite occurrences located in Devonian carbonate formations of the Axial Zone are known, for example in Salau, Aurenere, Costabonne, or les Tourrettes (Fig. 1).

Fig. 1 **a** Simplified geological map of the Paleozoic domain in the Pyrenees (southern France) modified from Denèle et al. (2011). **b** Regional structural scheme of the Salau area modified from Colchen et al. (1997)

Local geology

Stratigraphy and tectonometamorphic evolution of the wall-rocks

In the Salau/Aurenere district, the Paleozoic stratigraphic succession forms a large-scale monocline (Charuau and Derré 1976; Derré et al. 1980; Fig. 1). From bottom to top, the following stratigraphic units are defined:

The Mont Rouch Formation (Early to Middle Ordovician) is a flysch complex reaching up to 2 km in thickness. It is followed by a monotonous series of graphitic and pyritic Silurian shales known to act regionally as a thrusting level underneath the more competent Devonian rocks. To the north,

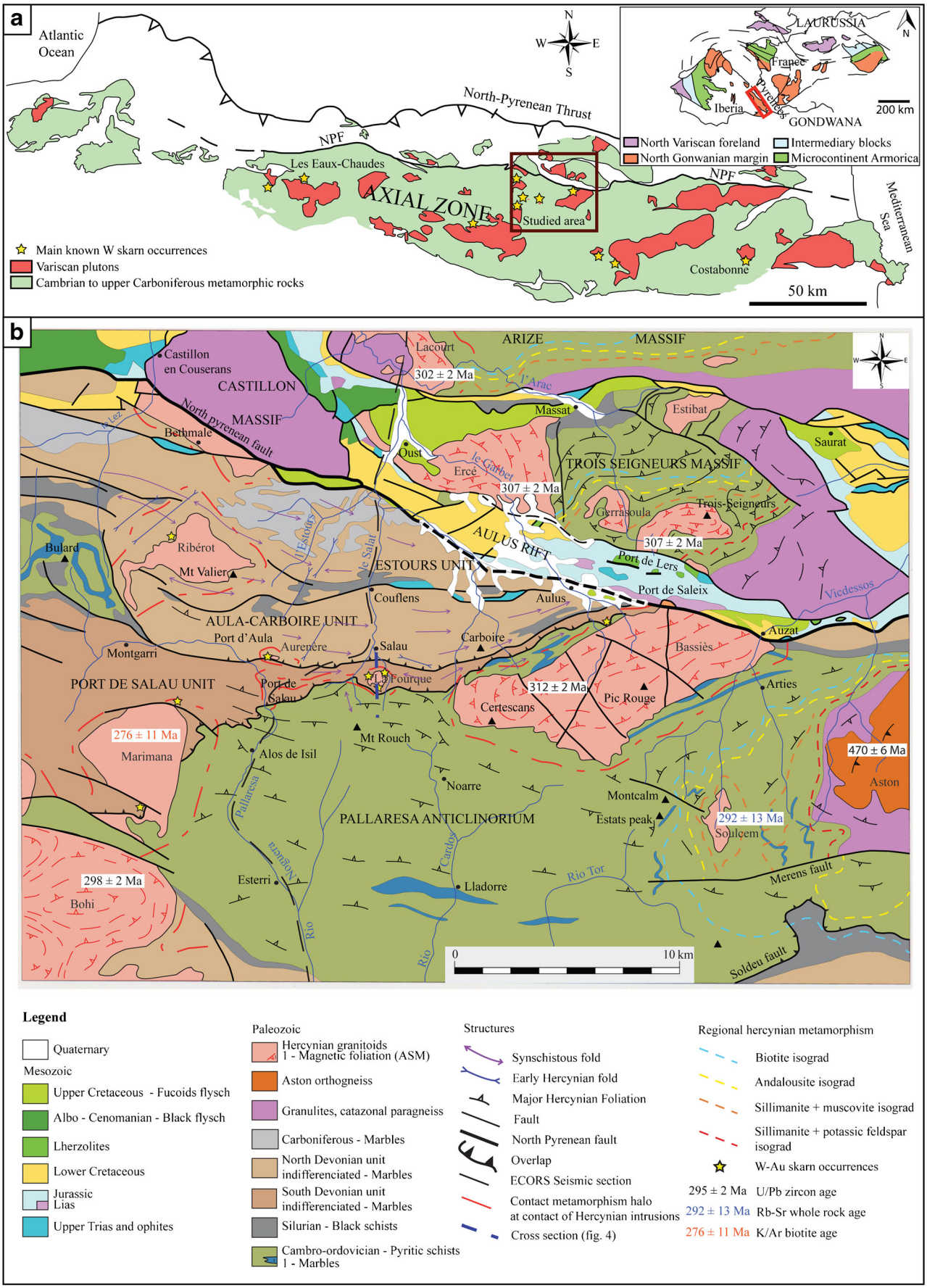
a
Atlantic Ocean
North-Pyrenean Thrust
NPF
Les Eaux-Chaudes
AXIAL ZONE
Studied area
Mediterranean Sea
Costabonne
50 km
Main known W skarn occurrences
Variscan plutons
Cambrian to upper Carboniferous metamorphic rocks
LAURUSSIA
France
Iberia
Pyrenees
GONDWANA
200 km
North Variscan foreland
North Gonwanian margin
Intermediary blocks
Microcontinent Armorica
b
ARIZE MASSIF
Lacourt
302 ± 2 Ma
Castillon en Couserans
CASTILLON MASSIF
North pyrenean fault
Bethmale
Massat
Estibat
Saurat
Oust
Ercé
TROIS SEIGNEURS MASSIF
307 ± 2 Ma
Gerrasoula
Trois-Seigneurs
AULUS RIFT
307 ± 2 Ma
Port de Lers
Port de Saleix
Vicdessos
Bulard
Ribérot
Mt Valier
ESTOURS UNIT
Couflens
Aulus
AULA-CARBOIRE UNIT
Port d'Aula
Aurenère
Salau
Carboire
Auzat
Montgarri
Bassiès
PORT DE SALAU UNIT
Port de Salau
Fourque
312 ± 2 Ma
Pic Rouge
Arties
Certescans
276 ± 11 Ma
Marimana
Mt Rouch
Alos de Isil
470 ± 6 Ma
Aston
Noarre
Montcalm
PALLARESA ANTICLINORIUM
Estats peak
292 ± 13 Ma
Soulcem
298 ± 2 Ma
Bohi
Esterri
Lladorre
Rio Tor
Merens fault
Soldeu fault
0
10 km
Legend
Quaternary
Mesozoic
Upper Cretaceous - Fucoids flysch
Albo - Cenomanian - Black flysch
Lherzolites
Lower Cretaceous
Jurassic Lias
Upper Trias and ophites
Paleozoic
Hercynian granitoids 1 - Magnetic foliation (ASM)
Aston orthogneiss
Granulites, catazonal paragneiss
Carboniferous - Marbles
North Devonian unit indifferenciated - Marbles
South Devonian unit indifferenciated - Marbles
Silurian - Black schists
Cambro-ordovician - Pyritic schists 1 - Marbles
Structures
Synschistous fold
Early Hercynian fold
Major Hercynian Foliation
Fault
North Pyrenean fault
Overlap
ECORS Seismic section
Contact metamorphism halo at contact of Hercynian intrusions
Cross section (fig. 4)
Regional hercynian metamorphism
Biotite isograd
Andalousite isograd
Sillimanite + muscovite isograd
Sillimanite + potassic feldspar isograd
W-Au skarn occurrences
295 ± 2 Ma U/Pb zircon age
292 ± 13 Ma Rb-Sr whole rock age
276 ± 11 Ma K/Ar biotite age

the Salau Formation comprises various carbonate and pelite intercalations. It consists of a lower member of graphitic limestones followed by centimetric alternations of siltstone and limestone beds. Near the top of the Salau Formation, the massive gray limestones occur. The top of the Salau Formation consists of bluish shales.

Three main tectonic stages of deformation have been distinguished in the study area (Derré et al. 1980), which correspond well with the regional tectonic evolution (Denèle et al. 2014; Cochelin et al. 2017). The first stage of deformation (D1) involved a top-to-the-SE shear deformation responsible for the development of recumbent isoclinal P1 folds of all dimensions whose axes have a consistent N45°E direction. These folds, which partially transpose the compositional layering, are associated with the development of a crenulation cleavage and a subhorizontal schistosity S1 (Déramond 1970; Charuau 1974; Derré 1979; Colchen et al. 1997; Denèle et al. 2014; Cochelin et al. 2017). The D2 deformation stage resulted in the formation of sub-vertical folds associated with epizonal regional metamorphism (greenschist facies 300–350 °C). P2 folds are isoclinal, hectometric in size, and overturned towards the North. Fold axis have a N110°E–N120°E direction. They are accompanied by a crenulation cleavage S2 parallel to their axial planes. The axial plane foliation (S2) is marked by muscovite and chlorite. This stage (D2) is also marked by the emplacement of the granodioritic apex, accompanied by contact metamorphism. The final D3 deformation stage is represented by large E–W (N80 to N120°E), steeply dipping (60 to 80°N), ductile shear zones and other brittle faults at the contact between the la Fourque granodiorite and the carbonate host rocks. These dextral reverse faults with a displacement of more than 200 m (Fig. 2; Lecouffe 1987) are characterized by strain folds in marbles, C–S structures in the granodiorite, and breccias.

Intrusive rocks

The La Fourque granodiorite crops out at the bottom of the Salat valley (Fig. 1). Its shape is almost equidimensional occupying an area of about 1 km^2. The morphology of the intrusive stock, established in an antiform, seems to be controlled by the regional structures defined by the thick carbonate formations surrounding it (Derré et al. 1984).

Kaelin (1982) and Soler (1977) showed that the granodiorite postdates the main foliation stage D2 (Denèle et al. 2014). The mylonites at the contact with carbonate country rocks are related to a more recent ductile–brittle or brittle deformation (Fonteilles et al. 1988).

Three main types of intrusive rocks can be distinguished in the vicinity of the Salau deposit: the apical marginal facies of the La Fourque granodiorite, a porphyritic facies in the centre of the intrusion, and aphanitic dykes or sills distinguished on the basis of their grain size, chemical, and mineralogical compositions (Toulhoat 1982; Guy 1988; ESM 1 Fig. 1). The marginal facies is a relatively dark, fine-grained granodiorite with an equigranular texture (0.5–1 mm) 100 to 250 m thick. It becomes thinner at depth where it disappears. This "apical granodiorite" is composed of interstitial crystalline quartz, plagioclase (An 20–60), rare microcline, abundant biotite, and accessory minerals (zircon, apatite). The chemical composition of the marginal facies corresponds to a granodiorite with a low K_2O content (2.6 wt%) compared to other granitoids in the upper Pyrenean massifs. The porphyritic facies in

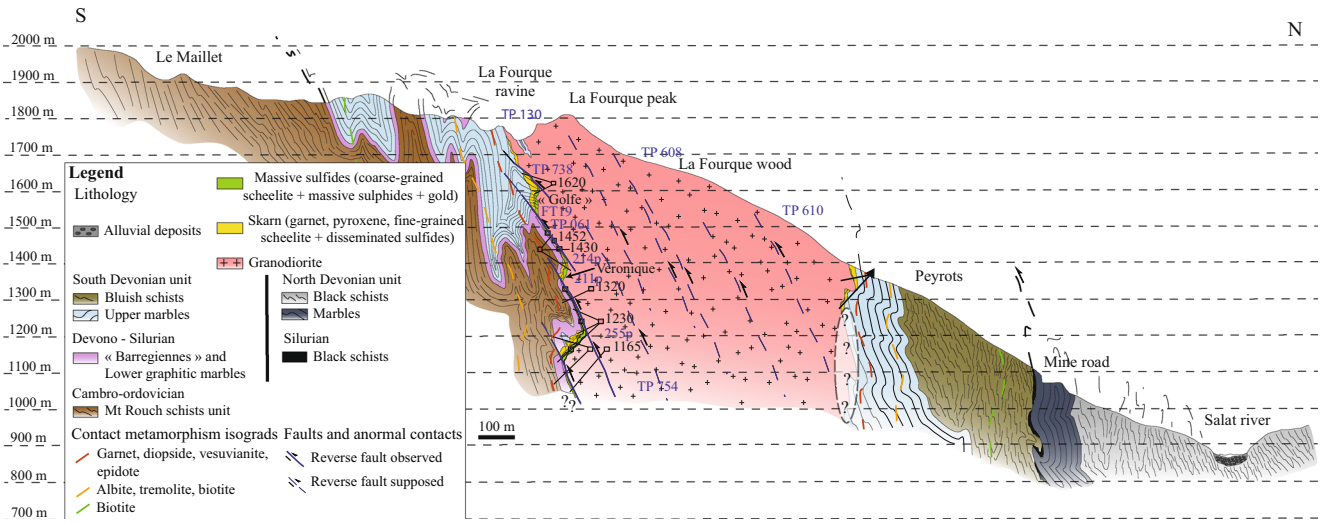

Fig. 2 North–south cross section of the La Fourque massif as constrained by field observations and drill hole data. Location of studied samples in blue. Note that metamorphic isograds cross the fold structure, which precedes the La Fourque granodioritic intrusion emplaced into a large-scale antiform. The massive sulfide ore is located along the Veronique Fault on the southern granodiorite border. Later, E–W 70°N faults displaced the ore for more than 100 m with a reverse movement

the center of the massif is a diorite–monzogranite, rich in potassium feldspar (20%) with higher K_20 (4.6 wt%). The two petrographic types belong to two different geochemical lineages (Raimbault and Kaelin 1987).

Different types of aphanitic sills and dykes are observed. Microdioritic dykes are cut by the apical granodiorite which contain dark microdiorite enclaves (Fonteilles et al. 1989). Aplite dykes cut both the La Fourque intrusive rocks and the marbles. They are commonly epidotized on the southern side of the La Fourque granodiorite.

The Aurenere W/Au occurrence crops out at 5 km to the West of the Salau deposit. The occurrence is also located at the contact between a granodioritic stock and Devonian marbles that are skarnified and mineralized over ca.100 m^2 (Fig. 1). The bulk chemical composition of the granodiorite stock is similar to that of La Fourque (ESM 1 Fig. 1), but, due to the erosion level, only the marginal facies is observed in the field. At its contact, the marbles are skarnified.

Mineralization styles

The first tungsten-bearing skarn was discovered in 1951, in contact with calc-alkaline intrusions at Costabonne in the Axial Zone of the Pyrenees (Guy 1988). The Salau deposit was discovered by in 1959, during regional tungsten exploration (Guiraudie et al. 1960). The deposit was estimated to contain 20,000 t of WO_3 from 1.3 Mt of ore at 1.5% WO_3 using a cutoff grade of 0.8 wt% WO_3 (Fonteilles et al. 1989). The orebodies located on the southern margin of the La Fourque granodioritic intrusion (Derré et al. 1980) were mined between 1970 and 1986 (Lecouffe 1987). The deposit was historically described as a scheelite skarn due to the presence of calcic silicates (grossular, hedenbergite) and because of its close spatial association with an intrusion. The deposit comprises two main orebodies, the Bois d'Anglade and the Veronique fault (Fonteilles et al. 1989). The Bois d'Anglade orebody is subdivided in three, named "Formation Nord," "Golfe," and "Formation Sud" (Fig. 2).

Two types of skarn were described at the Salau deposit (Derré et al. 1984). The first is massive and resulted from the transformation of the lower graphitic marbles or the upper marbles. It is often characterized by an almost monomineralic gangue mineralogy of either garnet or pyroxene. This first skarn does not carry significant tungsten mineralization. In contrast, the second skarn formed by metasomatism of calcic hornfels consists of alternating garnet-, pyroxene-, epidote-, and titanite-rich bands. These banded zones are inherited from the pre-existing sedimentary bedding.

A massive sulfide body of pyrrhotite, chalcopyrite, and sphalerite of 500 m × 250 m and 5 m thick is spatially associated to the Veronique Fault at the southern contact of the granodiorite with the country rocks. It is considered as part of the retrograde stage of the skarn (Fonteilles et al. 1989).

Mineralization at the Aurenere W/Au occurrence is similar to the Salau deposit. A grossular–hedenbergite–wollastonite skarn was formed during the prograde stage, whereas low contents of scheelite and disseminated sulfides (pyrrhotite, arsenopyrite) were developed during the retrograde stage. Late quartz veins cut skarn mineralization and contain coarse-grained scheelite and a massive arsenopyrite, pyrrhotite, chalcopyrite, sphalerite, and electrum (Palau i Ramirez et al. 1995; Palau i Ramirez et al. 1997; Palau i Ramirez 1998).

Field observations and mineralogy

The Bois d'Anglade orebody is crosscut by the Veronique Fault along its southern edge (Fig. 3a). The Bois d'Anglade orebody displays a comb shape located in an embayment of the Salau granodiorite. The bedding of Devonian-aged metasedimentary host rocks (N80E 80°N) is perpendicular to the contact with the intrusion in the embayment.

The Formation Nord and the Golfe orebodies consist of skarn (Fig. 3b) containing fine-grained scheelite. The prograde stage of skarn consists of a grossular, hedenbergite, and fine-grained scheelite (< 50 μm) assemblage (Fig. 4a). During the retrograde stage, garnet was replaced by epidote, whereas hedenbergite was replaced by amphibole, accompanied by the deposition of disseminated arsenopyrite and pyrrhotite (Fig. 4f). The proximal zone (up to 30 m from the intrusion) consists of garnet, pyroxene, and scheelite. The distal zone is characterized by a wollastonite-bearing assemblage. In this zone, the scheelite size is mostly fine-grained and less abundant.

In contrast, the Formation Sud orebody located along the strike of the Veronique Fault, which intersects the contact between the granodiorite and the marble (Fig. 3d), consists mainly of massive sulfides without skarn (Fig. 3c). Along the strike of the fault, the granodiorite is altered (albitized and chloritized) and brecciated with mylonitic clasts (Fig. 3e). The massive sulfides hosted by the Veronique Fault consist of coarse-grained scheelite, euhedral apatite, massive pyrrhotite, arsenopyrite, chalcopyrite, sphalerite, native bismuth, electrum (80% Au, 20% Ag), laitakarite, and tetrahedrite (Fig. 4b). Scheelite is coarse-grained (0.2–1 cm) with poikilitic crystals cut by late sulfides (Fig. 4c). Arsenopyrite was the first mineral to appear in this assemblage. It is fractured and filled by late pyrrhotite, chalcopyrite, and sphalerite accompanied by the crystallization of euhedral apatite, native bismuth, electrum, laitakarite, and tetrahedrite (Fig. 4e). Apatite grains are euhedral and unaltered. (Fig. 4h). Then, late veins of quartz, scheelite, calcite, and powdery chlorite cut the sulfides and represent the last stage of ore formation.

In the Formation Nord and Golfe orebodies, similar massive sulfides form lenses or clusters in the garnet and pyroxene skarn along the bedding of the country rocks or near the contact with the granodiorite. Strain folds, C–S structures and sigma clasts in skarn, cemented by massive sulfides along

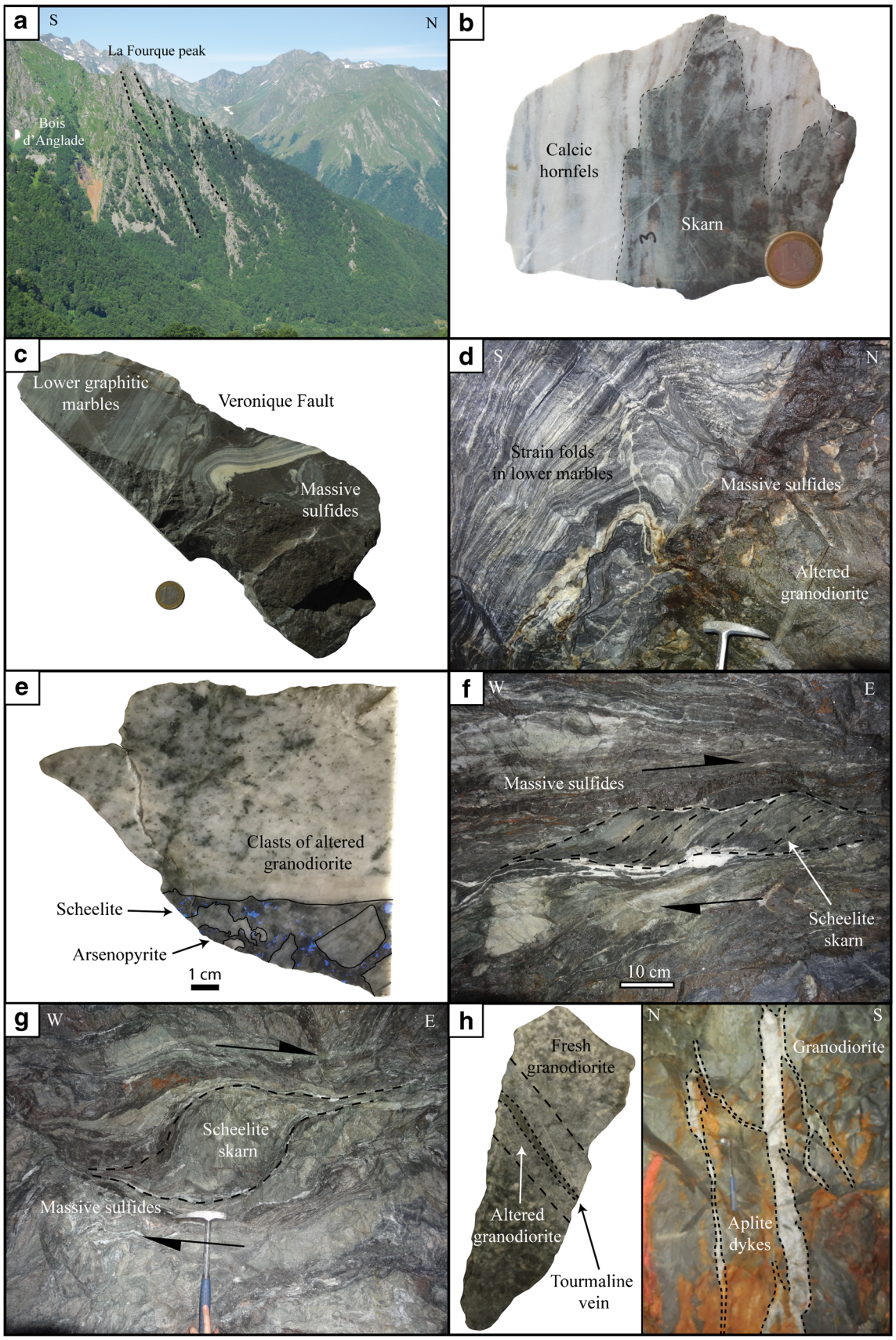
a
S
N
La Fourque peak
Bois d'Anglade
b
Calcic hornfels
Skarn
c
Lower graphitic marbles
Veronique Fault
Massive sulfides
d
S
N
Strain folds in lower marbles
Massive sulfides
Altered granodiorite
e
Clasts of altered granodiorite
Scheelite
Arsenopyrite
1 cm
f
W
E
Massive sulfides
Scheelite skarn
10 cm
g
W
E
Scheelite skarn
Massive sulfides
h
Fresh granodiorite
Altered granodiorite
Tourmaline vein
N
S
Granodiorite
Aplite dykes

◀ **Fig. 3** Field photographs showing the following: **a** general view of La Fourque intrusion with late faults; **b** sample of calcic hornfels skarnified in an embayment with comb teeth texture; **c** sample of deformed lower marble collected along the Veronique Fault with massive sulfides; **d** drag folds developed in the lower marble along the Veronique fault at contact with the La Fourque granodiorite; **e** altered granodiorite breccia along the Veronique Fault, cemented by massive sulfides and coarse-grained scheelite; **f** C–S structures in sheared skarn along the Veronique shear zone showing an east–west direction and a reverse movement; **g** sigma structure of skarn in the Veronique Fault showing an east–west direction and a reverse movement; **h** La Fourque granodiorite cut and altered by tourmaline veinlet and decimetric aplite dykes cutting the altered granodiorite

the contact between the fault and the granodiorite indicate dextral reverse kinematics (Fig. 3f, g). Aplitic dykes are locally spatially associated with the massive sulfide mineralization and crosscut the La Fourque granodiorite and the scheelite skarn (Fig. 3h). In some places, tourmaline veins, spatially related to massive sulfides, cut and alter the granodiorite (Fig. 3h; Lecouffe 1987). The skarn ore is intersected and displaced with a reverse kinematic at the contact with ductile, quartz-bearing, N90E 70°N faults. All around the La Fourque stock, sulfides are disseminated in hydrothermally altered granodiorite. All these features indicate that the massive sulfides formed after the la Fourque intrusion (Fig. 5).

Cathodoluminescence imaging

Cathodoluminescence imaging (Tescan, BRGM Orleans) was realized on selected zircon, apatite, and scheelite grains in order to detect inherited cores or zoning. Zircon grains from the Salau and Aurenere granodiorite do not show inherited cores (ESM 1 Fig. 2a, c and e; Fig. 5), with the exception of two grains (sample TP709 and TP728, ESM 1 Fig. 2b and 2d). Magmatic apatite is poikilitic and altered as droplets with growth zoning (TP 130, TP 608 and TP728, ESM 1 Fig. 3c and d). Hydrothermal apatite is euhedral, unaltered, sometimes with complex zoning, and contrast difference between core and rim (FT19, TP061, and TP 738; ESM 1 Fig. 3a and b). However, given its rhythmic aspect perpendicular to the rim, this contrast difference does not correspond to the presence of an inherited core but rather to compositional changes during the growth of the crystals. Finally, scheelite grains show growth zones without any evidence for inheritance (ESM 1 Fig. 4a, b, c; Fig. 9d).

Mineral chemistry of scheelite and apatite

Materials and methods

Fifty scheelite and 21 apatite grains were selected on thin and polished sections from 8 samples from the intrusive rocks and the two different types of mineralization. The location of the samples is given on Fig. 2. The data set is given in ESM 2 Tables 1 and 2.

LA-ICP-MS analyses were performed at Brest University (France) in order to obtain REE data for scheelite and apatite as well as Mo and W contents in scheelite, using a Geolas 193-nm Excimer Laser coupled to a Thermo Element II ICP-MS. Analytical conditions for the laser include a frequency of 10 Hz, a fluence of 6 J/cm^2, and a spot size of 40 μm. Ablated material is transported to the ICP-MS in a helium flux of 253 mL/min. The mass spectrometer is initially calibrated with a multi-element solution. Reference standard is NIST 612, and the quality control standards are BIR 1 and BCR 2. A batch of analyses comprises a sequence of NIST 612, BIR 1, and BCR 2 standards followed by 20 samples. Raw data were processed using Glitter (Van Achterbergh et al. 2001) to obtain atomic concentrations. Ca^{43} was used as the internal standard. REE concentrations were normalized to chondrite (McDonough and Sun 1995).

Results

Early fine-grained scheelite has a higher content in Mo (75–240 ppm) than the late coarse-grained scheelite (0–70 ppm; Fig. 6).

Magmatic apatite shows a relatively flat REE pattern with a prominent negative Europium anomaly (Fig. 7a) with Eu/Eu* and Ce/Ce* values ranging from 0.03 to 0.08 and 0.88 to 1.03, respectively (Fig. 8a). A similar REE distribution is observed for fine-grained scheelite from Salau and Aurenere, with a large negative Europium anomaly (Fig. 7b, c). Eu/Eu* and Ce/Ce* ratios yield similar values ranging between 0.06–0.14 and 0.89–1.07 for Salau and 0.4–0.55 and 0.76–0.87 for Aurenere, respectively (Fig. 8a)

Hydrothermal apatite crystals, which are texturally cogenetic with the massive sulfides, show two types of REE patterns, correlated with inner textures of the grains. Core of grains (ESM 1 Fig. 3a and b) are enriched in light REE, depleted in heavy REE with a moderate negative Europium anomaly (Fig. 7d). Rims of the same apatite grains (ESM 1 Fig. 3a and b) are also enriched in light REE and depleted in heavy REE but present a positive Europium anomaly (Fig. 7d). Eu/Eu* and Ce/Ce* returned values of 0.22–6.4 and 0.74–1.05, respectively (Fig. 8a) and therefore plot out of the domain of magmatic apatite.

Coarse-grained scheelite from massive sulfides contemporaneous of hydrothermal apatite presents an enrichment in light REE (except La and Ce) and a depletion in heavy REE with small or absent Eu anomalies (Fig. 7e). These scheelite grains yield very different Eu/Eu* ratios from hydrothermal apatite ranging from 0.6 up to 1.48 for Ce/Ce* showing low variation around 0.81–1.03 (Fig. 8b). Late scheelite crystals found in quartz–calcite–chlorite veins and have a REE chemistry similar to the rims of the apatite grains in the massive

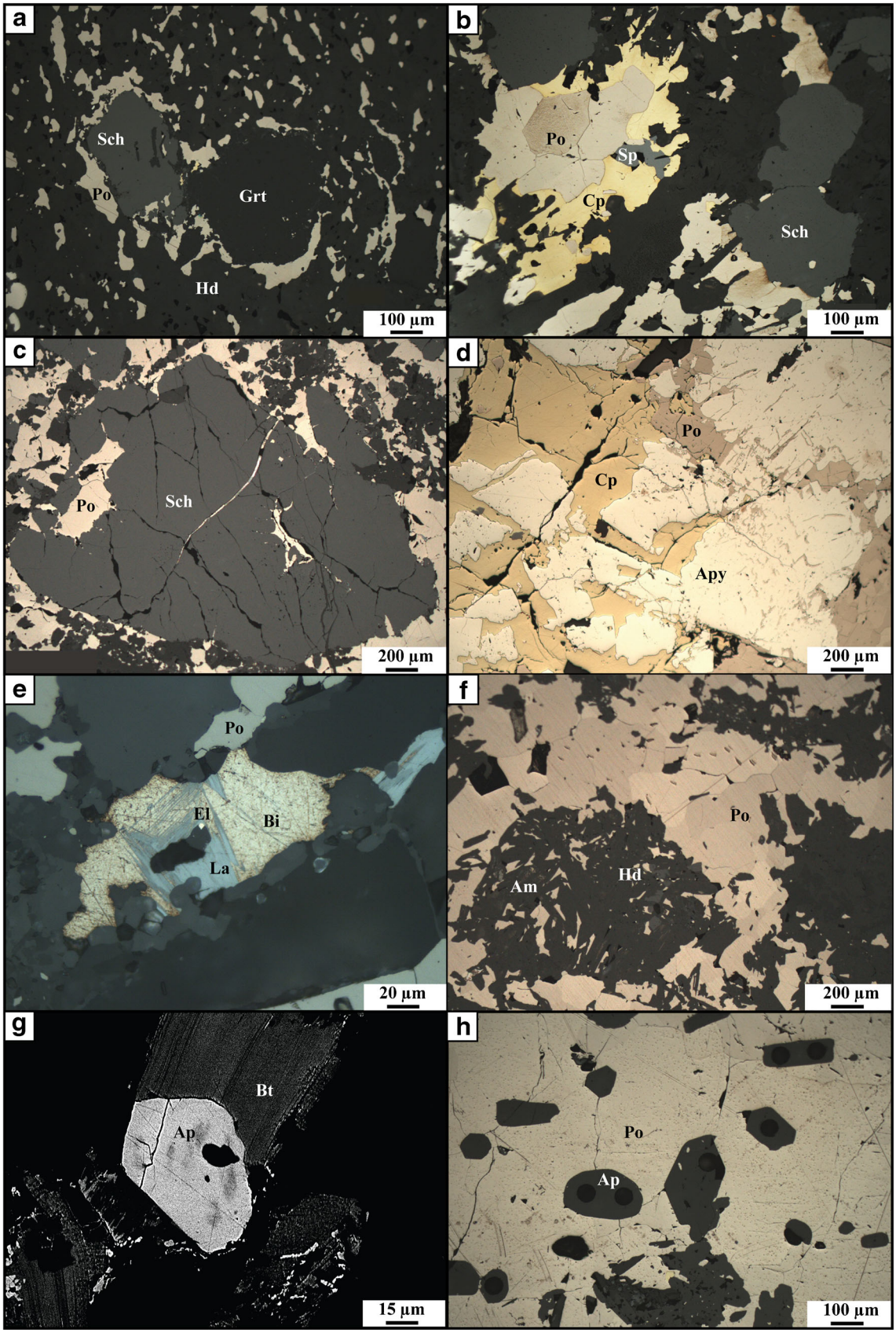
a
Sch
Po
Grt
Hd
100 μm
b
Po
Sp
Cp
Sch
100 μm
c
Po
Sch
200 μm
d
Po
Cp
Apy
200 μm
e
Po
El
Bi
La
20 μm
f
Po
Am
Hd
200 μm
g
Bt
Ap
15 μm
h
Po
Ap
100 μm

◀ **Fig. 4** Thin section microphotographs illustrating the following: **a** disseminated pyrrhotite associated with fine-grained scheelite and grossular garnet in skarn bedding; **b** massive sulfides paragenesis with an assemblage of pyrrhotite–chalcopyrite–sphalerite crosscutting the coarse scheelite; **c** coarse-grained scheelite fragmented and cemented by massive pyrrhotite; **d** arsenopyrite crystals fragmented and cemented by chalcopyrite and massive pyrrhotite; **e** native bismuth–laitakarite–electrum assemblage typical of Salau gold paragenesis; **f** hedenbergite replaced by amphibole, intergrown with massive pyrrhotite; **g** back scattered electron image of fragmented magmatic apatite contemporaneous with biotite in La Fourque granodiorite; **h** contemporaneous of massive pyrrhotite and hydrothermal, euhedral apatite

sulfide ores (Fig. 7f, g) with slightly higher Ce/Ce* ratios reaching ca. 0.9–1.15. Very coarse-grained scheelite has two REE patterns: one is similar to late scheelite, the other is enriched in LREE (Fig. 7g).

LA-ICP-MS U/Pb geochronology

Materials and methods

Zircon, apatite, and scheelite grains were selected from 12 samples issued from the intrusive rocks and the two different types of mineralization. The location of the samples is provided on Fig. 2. Raw data is given in ESM 2 Tables 3, 4, and 5. Five fresh samples of igneous rocks were selected for U/Pb dating on zircon, three samples from the La Fourque intrusion (TP 754, TP 608, TP 610), and two samples from the Aurenere intrusion (TP 728, TP 709). Four samples were selected for U/Pb dating on apatite. One sample (TP 130) is magmatic apatite from the marginal facies of the La Fourque granodiorite. Three samples (TP 061, FT19, TP 738) are hydrothermal apatite associated with coarse-grained and massive

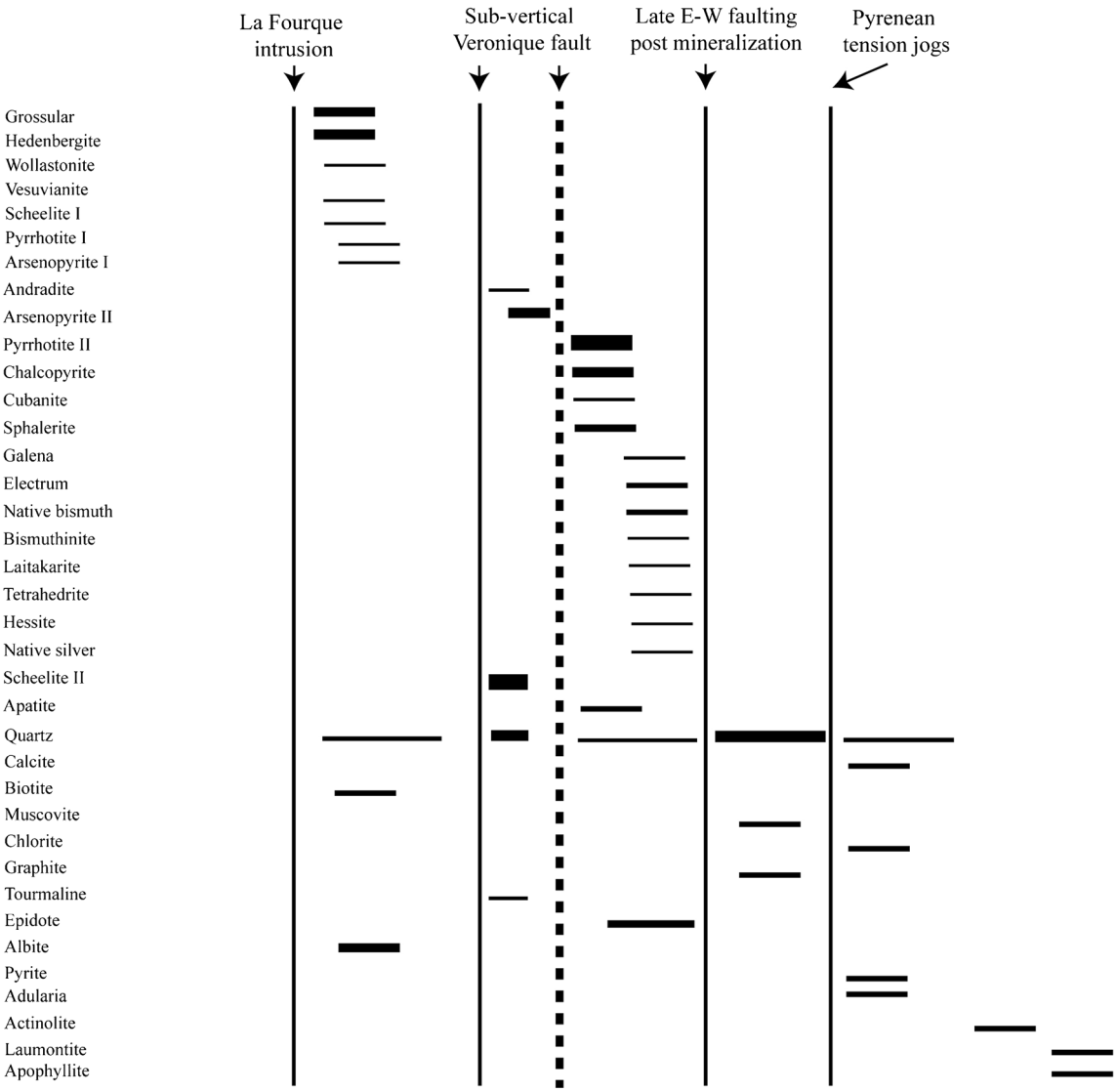

Fig. 5 Paragenetic sequence of the Salau W/Au–Cu deposit. Three main stages are distinguished, the scheelite skarn, the massive sulfide ore, and late alteration

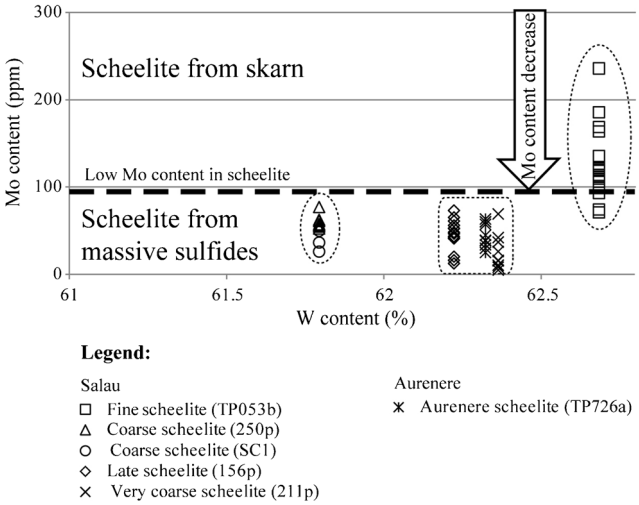

Fig. 6 Diagram of molybdenum grade (ppm) vs tungsten content (%) in function of different scheelite types analyzed by LA-ICPMS. Fine-grained scheelite shows higher molybdenum content (80–250 ppm) than coarse-grained scheelite (5–80 ppm) for the Salau deposit

sulfides. Three samples of coarse-grained scheelite contemporaneous to the massive sulfide ore hosted by the Veronique fault were selected for U/Pb dating.

A classic mineral separation procedure was applied to concentrate the zircon grains using the facilities available at ISTO laboratory. Rock samples were crushed, and the fractions with a particle size below 250 μm were processed further. Heavy minerals were concentrated by heavy liquids from the size fraction. Magnetic minerals were then removed with an isodynamic Frantz magnetic separator. Zircon grains were carefully handpicked under a binocular microscope and embedded in epoxy mounts that were then polished. For apatite and scheelite, U/Pb dating was realized in context on regular thin sections. U/Pb geochronology was conducted in situ by laser ablation inductively coupled plasma mass spectrometry (LA-ICP-MS) at Geosciences Rennes using an ESI NWR193UC Excimer laser coupled to an Agilent 7700x quadrupole ICP-MS equipped with a dual pumping system to enhance sensitivity (Paquette et al. 2014). The instrumental conditions are reported in ESM 2 Table 6. Additional information about the protocols used for U/Pb zircon dating can be found in Ballouard et al. (2015), and in Pochon et al. (2016) for apatite. According to Horstwood et al. (2016), uncertainties obtained for the reference material Plesovice were propagated to the analyzed zircon grains.

For U–Pb dating of scheelite, we followed the protocol of Wintzer et al. (2016) and used the NIST 612 glass standard as our primary standard (see ESM 2 Table 6). For all the samples, results are plotted in Tera-Wasserburg diagrams using Isoplot/Ex (Ludwig 2012). All errors are provided at 1σ level for zircon and 2σ level for apatite and scheelite.

Results

Zircon dating

Sample TP 754 is from the marginal facies at the SE edge of the La Fourque intrusion. Twenty-one zircon grains were analyzed (ESM 2 Table 3; Fig. 9a). Thirteen of these analyses are concordant (Fig. 9a) and define a concordia date of 295 ± 2.4 Ma (MSWD = 0.57). Five analyses either in zircon cores or in homogeneous grains define inherited apparent ages from older material around 325 and 350 Ma. Finally, 6 analyses are sub-concordant to discordant and are interpreted as reflecting the presence of a small amount of common Pb together with a slight Pb loss.

Sample TP 608 was collected in the porphyritic facies of the La Fourque intrusion. Eighteen zircon grains were analyzed (ESM 2 Table 3; Fig. 9b). Seven of these analyses (Fig. 9b) are concordant and yield a Concordia date of 296.9 ± 3.2 Ma (MSWD = 1.4) interpreted as the age of the intrusion. The remaining data are discordant at 280 Ma and attributed to Pb loss.

Sample TP 610 was collected on the northern side of the La Fourque intrusion from porphyritic facies. Twenty-four zircon grains were analyzed (ESM 2 Table 3; Fig. 9c). Fifteen analyses are concordant and yield a concordia date of 294.5 ± 2.2 Ma (MSWD = 0.81; Fig. 9c) interpreted as the emplacement age for this granodiorite. One concordant analysis yields an inherited apparent age from older material of ca. 320 Ma. Six analyses are discordant perhaps because of Pb loss and/or the presence of common Pb. In summary, all three samples from the La Fourque granodiorite yield concordant ages comparable within error at ca 295 Ma.

TP 709 and TP 728 were sampled on the Aurenere granodioritic intrusion. For sample TP 709, nineteen analyses were performed (ESM 2 Table 3; Fig. 9d). Nine of them are concordant (Fig. 9d) and yield a Concordia age of 293.9 ± 2.8 Ma (MSWD = 0.29). Twelve discordant results show either older, inherited, apparent ages, or Pb loss. On sample TP 728, eighteen analyses are concordant and yield a Concordia age of 293.4 ± 2 Ma (MSWD = 1.13) (ESM 2 Table 3; Fig. 9e). Two analyses define older inherited apparent ages from older material at ca. 700 and 570 Ma while one analysis shows signs of Pb loss. Therefore, all these results agree for an emplacement age at ca. 295 Ma for the Aurenere intrusion, indistinguishable from the emplacement age of the La Fourque intrusion.

Apatite dating

For sample TP 130, seventeen grains that were analyzed (ESM 2 Table 4) are discordant position (Fig. 10b) with a lower intercept of 297.3 ± 7.1 Ma (MSWD = 6.7).

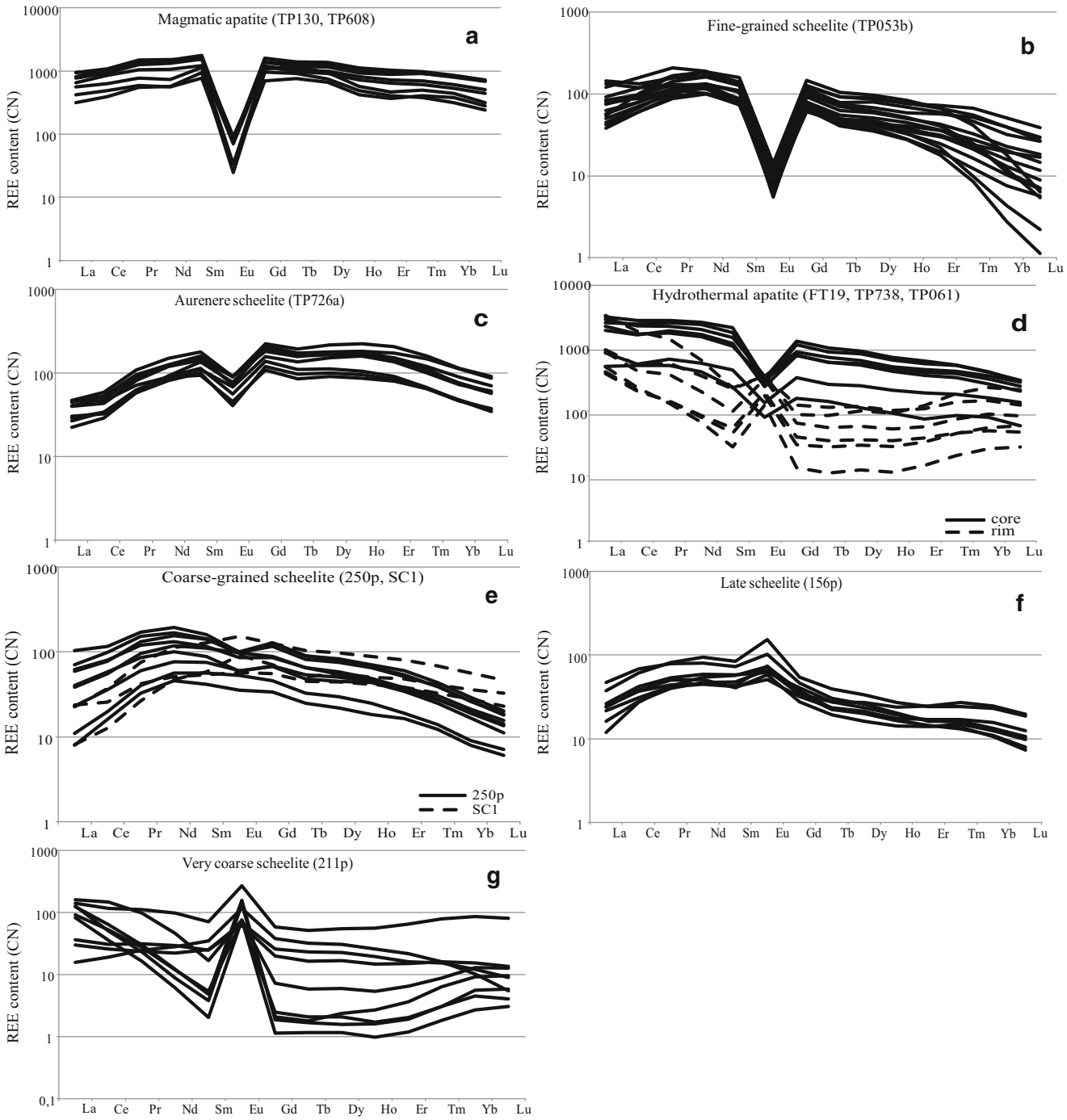

Fig. 7 Comparison of REE spectra for different apatites and scheelites analyzed by LA-ICPMS. Magmatic apatite from Salau and fine-grained scheelite from Salau and Aurenere shows a similar relatively flat REE pattern with a strong negative europium anomaly (**a**–**c**). Hydrothermal apatite from Salau and Aurenere recorded an enriched LREE spectrum with negative europium anomaly in core and positive one on border (**d**). Coarse-grained scheelite from Salau displays an enriched LREE pattern with a positive europium anomaly (**e**–**g**)

Hydrothermal apatite grains were collected in massive sulfides of the Golfe (TP 061), the Formation Sud (TP 738), and the Veronique Fault (FT19). All the apparent ages obtained on these apatites are similar within error (Fig. 10a, c, d) if discordia are forced to a common Pb composition of $^{207}Pb/^{206}Pb = 0.870$ obtained on galena from the massive sulfide mineralization (Marcoux and Moëlo 1991; Chew et al. 2014; Cochrane et al. 2014): TP 061 yields an age of 278 ± 9.7 Ma ($N = 17$; MSWD = 0.25), TP 738 gives a date of 287 ± 4.6 Ma ($N = 15$; MSWD = 3.2), and FT19 yields a date of 288.2 ± 3.4 Ma ($N = 16$; MSWD = 21). If all these data are plotted together in the same Tera-Wasserburg diagram

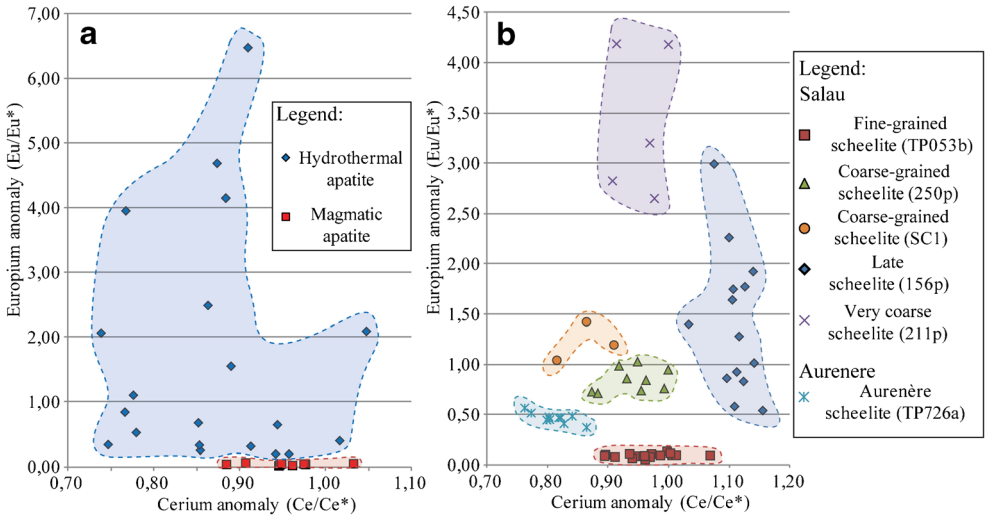

Fig. 8 Ce/Ce* vs Eu/Eu* anomalies diagram for apatite (a) and scheelite (b), adapted from Mao et al. (2016). Anomaly values were calculated using Eu/Eu* = EuCN/(SmCN·GdCN)$^{0.5}$ and Ce/Ce* = CeCN/(LaCN·PrCN)$^{0.5}$ (Worrall and Pearson 2001). CN: normalized data to chondrite (McDonough and Sun 1995)

(Fig. 10e), they return a date of 289.1 ± 1.9 Ma (N = 48; MSWD = 9.2).

Scheelite dating

Discordia ages were calculated for the coarse-grained scheelite (100 μm–2 mm) from Salau (211p, 214p, and 255p) (Fig. 10f, g h). Only scheelite from sample 255p contains sufficient uranium for dating (Fig. 10h). Sample 255p from Veronique Fault (n = 56; MSWD = 8.6) yields an age of 284 ± 11 Ma (2σ) when forced to $^{207}Pb/^{206}Pb$ = 0.870 (Marcoux and Moëlo 1991). Data with slight Pb loss were not taken into account for the calculation. Other samples returned poorly constrained ages of 256 ± 28 Ma (2σ) (214p) and 262 ± 16 Ma (2σ) (211p).

Discussion

In contrast to several skarn deposits worldwide, the Salau deposit has the particularity to host two different types of mineralization. The combination of field observations with mineral chemistry and geochronology provides insights to decipher the evolution stages of the mineralization.

Nature of the fluids

The mineral chemistry of scheelite and apatite provides evidence for mineral formation from different fluid sources. Higher Mo contents in the paragenetically early, skarn-hosted scheelite (Fig. 6) are in a good agreement with observations made on other deposits, such as Los Santos (Timon Sanchez et al. 2009), Mittersill (Eichhorn et al. 1999), Costabonne (Raimbault et al. 1993), or Eastern China (Song et al. 2014; Poulin et al. 2018). The lower Mo contents found for the paragenetically late, coarse-grained, scheelite could suggest formation from a fluid depleted in Mo.

REE data for cogenetic scheelite and apatite that provide further evidence for distinct mineralizing events (Raimbault et al. 1993) were two groups of REE patterns and are recognized for both scheelite and apatite, suggesting that two fluids are associated with mineralization. The first group of REE patterns is relatively flat, with a distinct negative Eu anomaly. Both the magmatic apatite of the La Fourque granodiorite (Fig. 7a) and fine-grained scheelite from the scheelite skarn (Fig. 7b) display these typical patterns for minerals derived from a magmatic source (Raju et al. 2015) which suggest they are linked here to the emplacement of the La Fourque granodiorite into Devonian marbles.

The second group of REE patterns is marked by LREE enrichment and moderate to high Eu/Eu* anomalies. Hydrothermal apatite grains present in the massive sulfide ore display negative europium anomalies in the core (Fig. 7c) and positive anomalies in rims (Fig. 7c). Cathodoluminescence images show contrasted growth bands (ESM 1 Fig. 3a and b) and confirm the compositional nature of the observed zonation. These compositional changes reflect the chemical evolution of the hydrothermal fluid. Coarse-grained scheelite, also associated with massive sulfides, presents a similar REE pattern with a weak positive Eu anomaly, as the typical signature of hydrothermal system (Lottermoser 1992).

Figure 11 shows the distribution of the different scheelite generations in a ternary LREE-MREE-HREE (Light Rare Earth Element - Medium Rare Earth Element - Heavy Rare Earth Element) diagram (Raju et al. 2015). The fine-grained scheelite has a strong enrichment in LREE and plots near the "skarn, porphyry W-Mo deposits" cluster, whereas scheelite from massive sulfides, enriched in both LREE

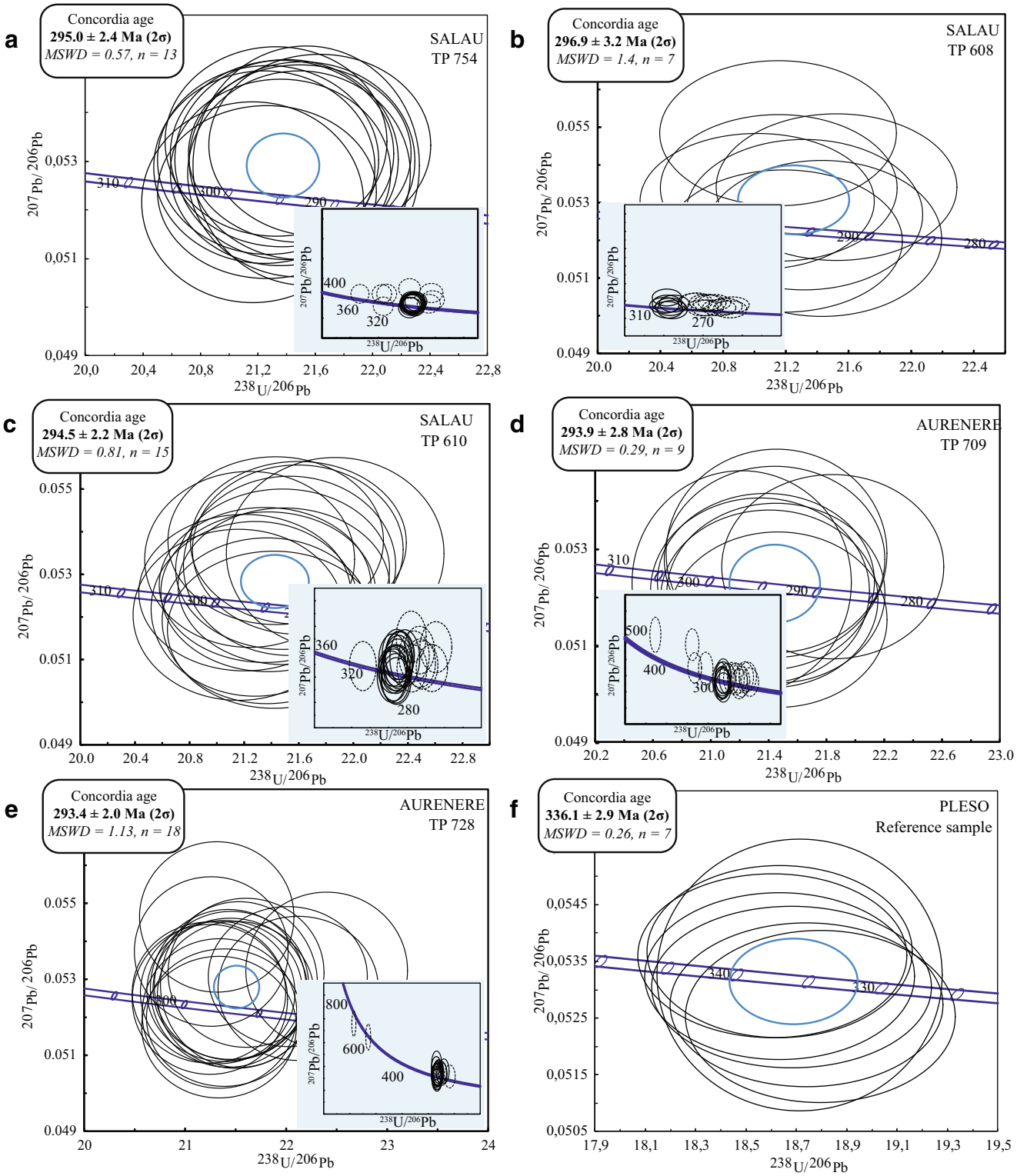

Fig. 9 Tera-Wasserburg concordia diagrams for zircon. **a-b–c** Salau granodiorite. **d**, **e** Aurenere granodiorite. **f** Pleso reference sample. N corresponds to the number of zircon grains that have been analyzed per sample. Ellipses and errors are reported at 2σ

and MREE, plots in the "vein Au-W deposits from West Australia" cluster. The discriminant diagram Eu/Eu* = f (Ce/Ce*) (Mao et al. 2016) also distinguishes these two groups for each mineral type (Fig. 8a, b). This likely reflects also the evolution of the fluid redox state. First, magmatic fluids from the La Fourque granodiorite, a reduced

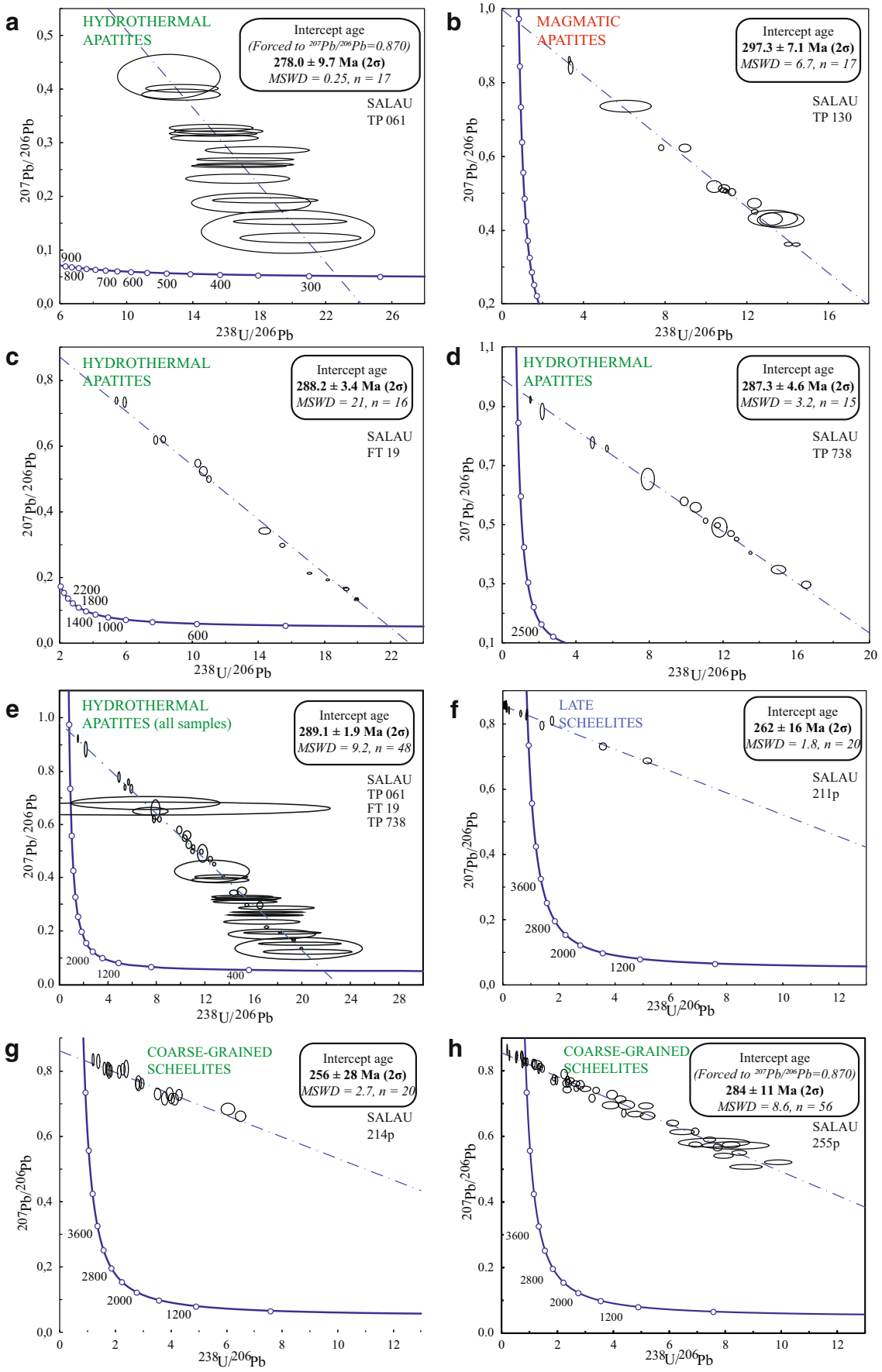
a
HYDROTHERMAL APATITES
Intercept age
(Forced to 207Pb/206Pb=0.870)
278.0 ± 9.7 Ma (2σ)
MSWD = 0.25, n = 17
SALAU
TP 061
b
MAGMATIC APATITES
Intercept age
297.3 ± 7.1 Ma (2σ)
MSWD = 6.7, n = 17
SALAU
TP 130
c
HYDROTHERMAL APATITES
Intercept age
288.2 ± 3.4 Ma (2σ)
MSWD = 21, n = 16
SALAU
FT 19
d
HYDROTHERMAL APATITES
Intercept age
287.3 ± 4.6 Ma (2σ)
MSWD = 3.2, n = 15
SALAU
TP 738
e
HYDROTHERMAL APATITES (all samples)
Intercept age
289.1 ± 1.9 Ma (2σ)
MSWD = 9.2, n = 48
SALAU
TP 061
FT 19
TP 738
f
LATE SCHEELITES
Intercept age
262 ± 16 Ma (2σ)
MSWD = 1.8, n = 20
SALAU
211p
g
COARSE-GRAINED SCHEELITES
Intercept age
256 ± 28 Ma (2σ)
MSWD = 2.7, n = 20
SALAU
214p
h
COARSE-GRAINED SCHEELITES
Intercept age
(Forced to 207Pb/206Pb=0.870)
284 ± 11 Ma (2σ)
MSWD = 8.6, n = 56
SALAU
255p
207Pb/206Pb
238U/206Pb

◀ **Fig. 10** Tera-Wasserburg concordia diagram for apatite and coarse scheelite. **a**, **c**, **d** Hydrothermal apatite from massive sulfides ore. **b** Magmatic apatite from the La Fourque granodiorite. **e** All hydrothermal apatite. N corresponds to the number of apatite grains that have been analyzed per sample. Ellipses and errors are reported at 2σ

intrusion (ilmenite series; Blevin 2004), compatible with disseminated pyrrhotite in the skarn, were recorded in fine grained scheelite (ESM 1 Fig. 5). More oxidized fluids are responsible for the formation of the coarse-grained scheelite, hydrothermal apatite, and massive sulfides as shown by the REE patterns. Combined with field observations, this implies mixing between oxidized meteoric fluids and the contribution of a second magmatic source, different from the granodiorite, to explain the massive sulfide deposition.

This interpretation is corroborated by isotopic studies and fluid inclusion data (Toulhoat 1982; Guy 1988) showing evidence for different stages of mineralization that coincide with a decrease in fluid temperature and evolution of hydrothermal fluid compositions. A first magmatic fluid, which contains H_2O and NaCl (Soler 1977), is found in the skarn minerals (quartz, garnet, hedenbergite, and scheelite). After the skarn formation, a H_2O–CO_2–CH_4 fluid was probably linked to the decarbonatation of the country rocks during metasomatism mixed with the magmatic fluid to precipitate scheelite (Krier-Schellen 1988). The parameters for the skarn formation are estimated at $470 < T°C < 530$, $-9 < \log fS2 < -6$, $-27.7 < \log fO2 < -21.1$ and $P \approx 2$ kbar (Soler 1977). For the massive sulfides, $\delta^{34}S$ values have been interpreted as characteristic of a fluid with a magmatic origin (Guy 1988; Palau i Ramirez 1998). The parameters for the late massive sulfide mineralization are estimated at $335 < T°C < 363$, $-9.51 < \log fS2 < -8.45$, $-32.8 < \log fO2 < -30.2$ and $2.16 < P$ (kbar) < 2.58 (Krier-Schellen 1988).

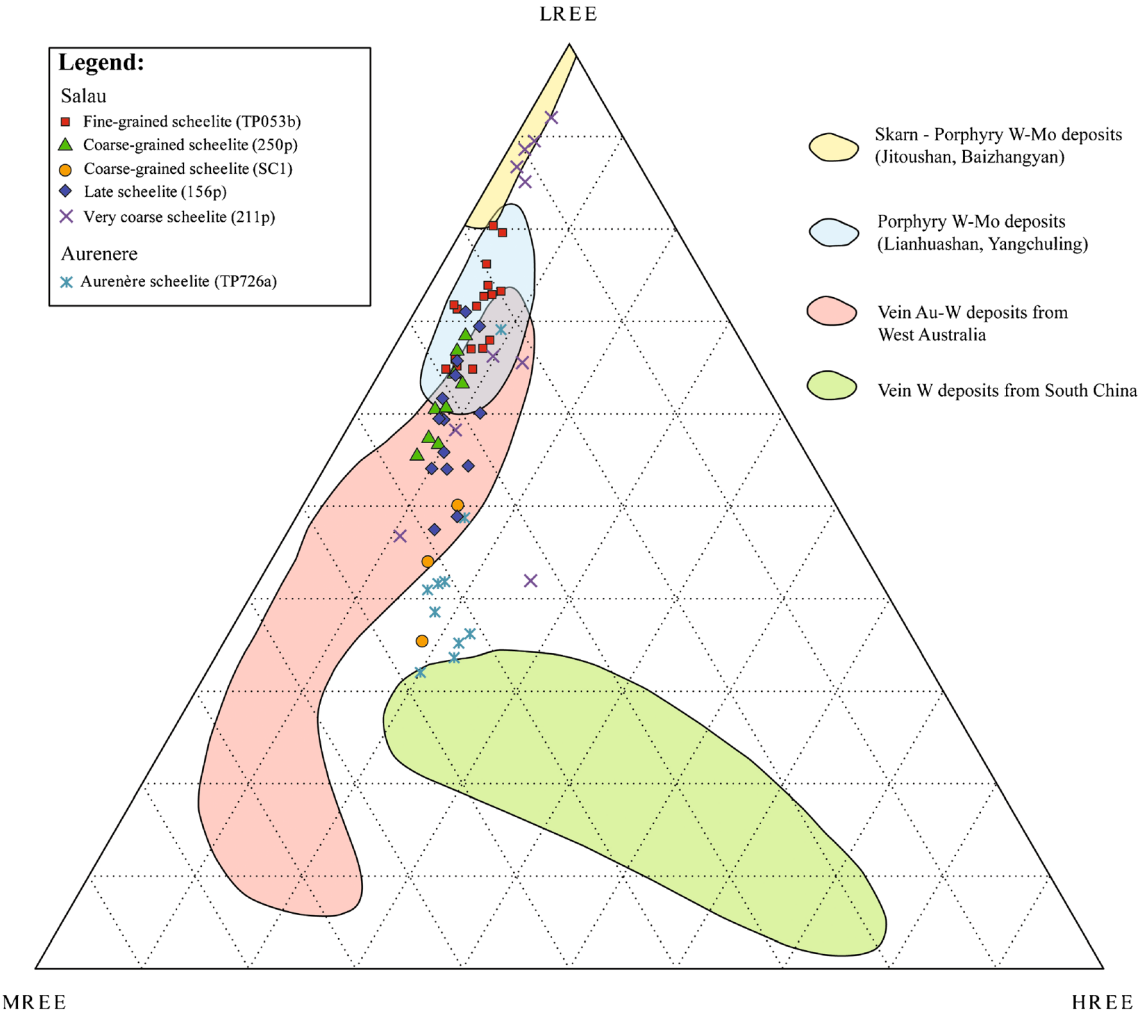

Fig. 11 LREE-MREE-HREE ternary diagram for the Salau and Aurenere scheelite analyzed by LA-ICPMS. (LREE = La + Ce + Pr + Nd, MREE = Sm + Eu + Gd + Tb + Dy, HREE = Ho + Er + Tm + Yb + Lu ; from Raju et al. 2015). The REE data of other scheelite were from Zhang et al. (1990), Sylvester and Ghaderi (1997), Ghaderi et al. (1999), and Song et al. (2014))

Absolute time constraints on the Salau/Aurenere W/Au deposit

Direct in situ U/Pb geochronology on zircon, apatite, and scheelite yields distinct ages for the different stages of ore formation. Zircon and magmatic apatite dating yields an age of ca. 295 Ma, corresponding to the emplacement age of the La Fourque and Aurenere intrusions. The associated massive skarns have the same age. Massive sulfide ores related to the Veronique Fault formed later, as suggested by an age of 289 ± 2 Ma for hydrothermal apatite. Coarse-grained scheelite from massive sulfide ore yields an age of 284 ± 11 Ma consistent with the hydrothermal apatite age. Using the emplacement age of the la Fourque intrusion at 295 ± 2 Ma (and related skarn) and 289 ± 2 Ma for the hydrothermal apatite associated with massive sulfides ore, it appears that these mineralizations are the result of two distinct metallogenic events separated by at least 2 Ma. This interpretation is in agreement with field relations (alteration features, tourmaline veins and breccias observed along the late shear zones), demonstrating that the deposition of the massive sulfide ore postdate granodiorite cooling (Fig. 3e–g).

A model for the cooling of the La Fourque intrusion, computed using Darcy's law and convection/conduction in porous media for an intrusion, was emplaced at 2 kbar. A geothermal gradient of 40 °C/km was used for the marble host rocks (Cochelin et al. 2017) and an initial temperature of 900 °C for the granodiorite. The permeability of the marble is set at 1.10^{-16} m^2 and that of the granodiorite is 1.10^{-19} m^2. In this example, the la Fourque granodiorite intrusive body (1 km^2) cooled to geothermal gradient in less than ca. 40,000 years, comparable to other values of ca. 200,000 years (Petford et al. 2000; Eldursi et al. 2009; Chauvet et al. 2012; Nabelek et al. 2012; Bucholz et al. 2017). This implies that it cannot be the source for the coarse-grained scheelite, massive sulfide, and gold mineralization as they form at least 2 Ma after the intrusion had cooled.

At Salau, where massive sulfide mineralization within shear zone has a magmatic origin according to $\delta^{34}S$ and fluid inclusions studies (Toulhoat 1982; Guy 1988; Krier-Schellen 1988), an igneous source other than La Fourque granodiorite is required. In Salau mine, evidence for possible intrusive bodies, younger than the La Fourque granodiorite, includes tourmaline veinlets and aplite veins (Fig. 3h). That could be derived from an evolved granite, emplaced deeper in the crust. This granitic stock could thus be considered as part of a long-lasting, multi-intrusion event that was emplaced during D3 deformation event and which was ultimately responsible for the scheelite bearing massive sulfide ores. Such relationships between different intrusive rocks were also observed in the nearby massifs of Marimanya (Palau i Ramirez 1998) and Cauterets (Reyx 1973). Similar observations were made at Hämmerlein (Lefebvre et al. 2018) or Los Santos in Spain (Timon Sanchez et al. 2009), where different granites were emplaced within a time gap of ca. 10 Ma. Throughout the Variscan Orogen, other examples of sulfide mineralization, consecutive to an early, mostly tungsten-rich mineralization, were described, such as Puy les Vignes (Harlaux et al. 2018) and Panasqueira (Codeço et al. 2017).

Concluding remarks

The Salau deposit is the expression of regional deformation and magmatism in the axial zone of the Pyrenees during the late Variscan evolution (Fig. 12). The La Fourque granodiorite was emplaced at ca. 295 Ma contemporaneously to D2 event, in compressional regime into the upper crust at ca. 2 kbar. The intrusion is associated with contact metamorphism and the formation of skarns along the intrusive contact. This event corresponds to a period where the upper crust of the Axial Zone was abnormally warm and the N-S compressive tectonic regime was marked by hectometric E–W trending folds. Later, at ca. 289 Ma with crust cooling, the deformation regime changed and was localized in shear zones along previously emplaced granitic stocks and gneiss domes. As a consequence, shear zones were developed at their contact with host rocks or within graphitic metasedimentary beds.

The Salau deposit consists of two types of mineralization. The first is a skarn with garnet, pyroxene, and fine-grained scheelite mineralization with disseminated arsenopyrite and pyrrhotite. The second type, a breccia, consists of a coarse-grained scheelite with abundant massive sulfide mineralization (arsenopyrite, pyrrhotite, chalcopyrite, sphalerite, sulfosalts, native bismuth, and electrum) located in a major fault. The skarn is related to the La Fourque granodiorite emplacement at ca. 295 Ma (zircon and magmatic apatite). The massive sulfides ore is related to a reverse dextral, E–W trending Veronique Fault developed at ca. 289 Ma (hydrothermal apatite and coarse-grained scheelite). This age result is the first direct dating of the D3 Variscan deformation event. This interpretation is corroborated by isotopic and fluid inclusion data, indicating that the massive sulfides and scheelite mineralization were formed by a buried younger intrusion.

At a larger scale, this study points out that magmatism and hydrothermal events are phenomena which take place on relatively short timescales, generally between ca. 10^4 to 10^6 years. Nevertheless, these events can be the expression of the regional evolution typically in late-orogenic stage,

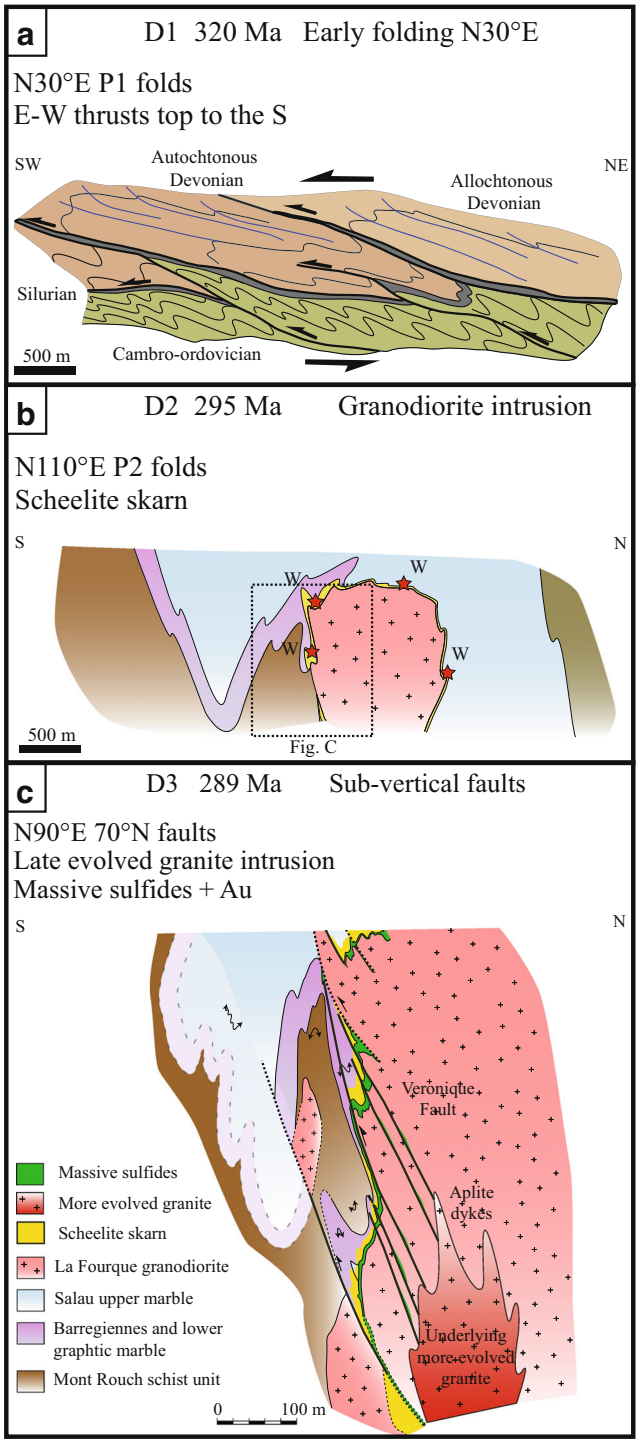

Fig. 12 Chronology of the Salau deposit genesis. **a** D1 corresponds to early folding N30°E. **b** D2 at ca. 295 Ma corresponds to the N–S compressional stage which led to N110°E folds formation, granodiorite intrusion and related scheelite skarn genesis. **c** Finally, D3 at ca. 289 Ma, a late evolved granite intrusion and the localization of deformation in shear zones during progressive cooling of the crust led to the formation of a scheelite, massive sulfides, and gold mineralization

extending over several millions of years, explaining the superimposed mineralization events.

Acknowledgments This investigation was supported by the society e-Mines through its R&D activity and the ISTO. The authors thank the following persons for their support on the field: F. Carbalido, F. Cheval-Garabedian, Q. Monge, J.L. Carbalido, and M. Bonnemaison. C. Derré, P. d'Arco, A.S. Audion, M. Picault, J. Gouin, G. Raoult, and B. Cochelin are thanked for their technical support including the provision of samples and valuable advice. I. Di Carlo (ISTO) is acknowledged for the MEB cathodoluminescence and microprobe analytical analyses. We particularly thank S. Janiec, G. Badin, and P. Benoist from ISTO laboratory for the thin sections and rock-crushing preparations. We also address our thanks to the IUEM (Brest) for LA-ICP-MS analyses. Finally, we would like to acknowledge the editor in chief G. Beaudoin, the associate editor J. Gutzmer, and two anonymous reviewers for their careful reading of this article and constructive remarks.

References

Aguilar C, Liesa M, Castineiras P, Navidad M (2014) Late Variscan metamorphic and magmatic evolution in the eastern Pyrenees revealed by U–Pb age zircon dating. J Geol Soc Lond 171: 181–192

Anglin CD, Jonasson IR, Franklin JM (1996) Sm-Nd dating of scheelite and tourmaline: implications for the genesis of Archean gold deposits, Val d'Or, Canada. Econ Geol 91:1372–1382

Autran A, Fonteilles M, Guitard G (1970) Relations entre les intrusions de granitoïdes, l'anatexie et le métamorphisme régional, considérées principalement du point de vue du rôle de l'eau: cas de la chaine hercynienne des Pyrénées orientales. Bull Soc Géol Fr 7:673–731

Ayora C, Casas JM (1995) Strata-bound As-Au mineralization in pre-Caradocian rocks from the Vall de Ribes, eastern Pyrenees, Spain. Mineral Deposita 21(4):278–287

Ballouard C, Boulvais P, Poujol M, Gapais D, Yamato P, Tartese R, Cuney M (2015) Tectonic record, magmatic history and hydrothermal alteration in the Hercynian Guérande leucogranite, Armorican Massif, France. Lithos 220–223:1–22

Ballouard C, Poujol M, Boulvais P, Mercadier J, Tartèse R, Venneman T, Deloule E, Jolivet M, Kéré I, Cathelineau M, Cuney M (2017) Magmatic and hydrothermal behavior of uranium in syntectonic leucogranites: the uranium mineralization associated with the Hercynian Guérande granite (Armorican Massif, France). Ore Geol Rev 80:309–331

Ballouard C, Poujol M, Mercadier J, Deloule E, Boulvais P, Cuney M, Cathelineau M (2018) Uranium metallogenesis in the peraluminous leucogranites from the Pontivy-Rostrenen magmatic complex (French Armorican Hercynian Belt): the result of long term oxidizing hydrothermal alteration during strike-slip deformation. Mineral Deposita 53:601–628. https://doi.org/10.1007/s00126-017-0761-5

Barnolas A, Chiron JC (1996) Synthèse géologique et géophysique des Pyrénées Edition BRGM – ITGE, p 1

Bechtel A, Elliot WC, Oszczepalski S (1996) Indirect age determination of Kuperfschiefer-type mineralization in the Polish Basin by K/Ar dating of illite; preliminary results. Econ Geol Bull Soc Econ Geol 91(7):1310–1319

Bell K, Anglin CD, Franklin JM (1989) Sm-Nd and Rb-Sr isotope systematics of scheelite: possible implications for the age and genesis of vein-hosted gold deposits. Geology 17:500–504

Blevin PL (2004) Redox and compositional parameters for interpreting the granitoid metallogeny of eastern Australia: implications for gold-rich ore systems. Resour Geol 54:241–252

Bodin J, Ledru P (1986) Nappes hercyniennes précoces à matériel dévonien hétéropique dans les Pyrénées ariégeoises. CR Acad Sci Paris 302(15):969–974

Bowles JFW (1990) Age dating of individual grains of uraninite in rocks from electron microprobe analysis. Chem Geol 83:47–53

Bozkaya O, Bozkaya G, Uysal IT, Banks DA (2016) Illite occurrences related to volcanic-hosted hydrothermal mineralization in the Biga Peninsula, NW Turkey; implications for the age and origin of fluids. Ore Geol Rev 76:35–51

Bucholz CE, Eddy MP, Jagoutz O, Bowring SA, Schmidt MW, Sambuu O (2017) Constraining the time scales of magmatic differentiation with U/Pb zircon geochronology. Geology 45(1):11–14

Cardellach E, Ayora C, Soler A, Delgado J, Stumpfi EF (1992) The origin of fluids involved in the formation of gold-bearing skarns of the Andorra granite (central Pyrenees, Spain); sulphur isotope data. Mineral Petrol 45(3–4):181–193

Carreras J, Capellà I (1994) Tectonics levels in the Palaeozoic basement of the Pyrenees: a review and a new interpretation. J Struct Geol 16(11):1509–1524

Casas JM, Domingo F, Poblet J, Soler A (1989) On the role of the Hercynian and alpine thrusts in the upper Paleozoic rocks of the Central and Eastern Pyrenees, Geodin. Acta 3(2):135–147. https://doi.org/10.1080/09853111.1989.11105181

Charuau D (1974) Relation entre les concentrations plombo-zincifères et la tectonique superposée du district de Hoque-Saubé-Carboire (Pyrénées ariégeoises). Thèse 3e cycle Paris VI

Charuau D, Derré C (1976) Place des minéralisations de plomb-zinc liées aux strates et des skarns à scheelite dans l'histoire structurale de la région de Carboire et Salau (Ariège, Pyrénées). Mémoire hors-série de la Société géologique de France 7:175–180

Chauvet A, Volland-Tuduri N, Lerouge C, Bouchot V, Monié P, Charonnat X, Faure M (2012) Geochronological and geochemical characterization of magmatic-hydrothermal events within the Southern Variscan external domain (Cévennes area, France). Int J Earth Sci 101:69–86

Che X, Wu F, Wang R, Gerdes A, Ji W, Zhao Z, Yang J, Zhu Z, Wang R, Zhou M (2015) In situ U/Pb isotopic dating of columbite-tantalite by LA-ICP-MS. Ore Geol Rev 65(4):979–989

Chesley J, Halliday A, Scrivener R (1991) Samarium–neodymium direct dating of fluorite mineralization. Science 252:949–951

Chesley J, Halliday A, Kyser T, Spry P (1994) Direct dating of Mississippi Valley-type mineralization; use of Sm–Nd in fluorite. Econ Geol 89:1192–1199

Chew DM, Petrus JA, Kamber BS (2014) U–Pb LA–ICPMS dating using accessory mineral standards with variable common Pb. Chem Geol 363:185–199

Christensen JN, Halliday AN, Leigh KE, Randell RN, Kesler SE (1995) Direct dating of sulphides by Rb-Sr: a critical test using the Polaris Mississippi Valley-type Zn-Pb deposit. Geochim Cosmochim Acta 59:5191–5197

Clauer N, Mercadier J, Patrier P, Laverret E, Bruneton P (2015) Relating unconformity-type uranium mineralization of the Alligator Rivers uranium field (Northern Territory, Australia) to the regional Proterozoic tectono-thermal activity; an illite K/Ar dating approach. Precambrian Res 269:107–121

Cochelin B, Lemirre B, Denèle Y, de Saint Blanquat M, Lahfid A, Duchêne S (2017) Structural inheritance in the Central Pyrenees: the Variscan to Alpine tectonometamorphic evolution of the Axial Zone. Journal of the Geological Society of London, published online first, 1st November 2017. https://doi.org/10.1144/jgs2017-066

Cocherie A, Rossi P, Fanning CM, Guerrot C (2005) Comparative use of TIMS and SHRIMP for U–Pb zircon dating of A-type granites and mafic tholeiitic layered complexes and dykes from the Corsican Batholith (France). Lithos 82(1–2):185–219

Cochrane R, Spikings RA, Chew D, Wotzlaw JF, Chiaradia M, Tyrrell S, Schaltegger U, Van der Lelij R (2014) High temperature (>350 °C) thermochronology and mechanisms of Pb loss in apatite. Geochim Cosmochim Acta 127:39–56

Codeço MS, Weiss P, Trumbull RB, Pinto F, Lecumberri-Sanchez P, Wilke FDH (2017) Chemical and boron isotopic composition of hydrothermal tourmaline from the Panasqueira W-Sn-Cu deposit, Portugal. Chem Geol 468:1–16

Colchen M, Ternet Y, Debroas EJ, Dommanget A, Gleizes G, Guérangé B, Roux L (1997) Carte géol. France (1/50 000), feuille Aulus-les-Bains (1086). BRGM

Decrée S, Deloule E, Ruffet G, Dewaele S, Mees F, Marignac C, Yans J, De Putter T (2010) Geodynamic and climate controls in the formation of Mio-Pliocene world-class oxidized cobalt and manganese ores in the Katanga province, DR Congo. Mineral Deposita 45: 621–629

Decrée S, Deloule E, De Putter T, Dewaele S, Mees F, Baele JM, Marignac C (2014) Dating of U-rich heterogenite: new insights into U deposit genesis and U cycling in the Katanga Copperbelt. Precambrian Res 241:17–28

Denèle Y, Olivier P, Gleizes G (2008) Progressive deformation of a zone of magma transfer in a transpressional regime: The Variscan Mérens shear zone (Pyrenees, France). J Struct Geol 30(9):1138–1149. https://doi.org/10.1016/j.jsg.2008.05.006

Denèle Y, Olivier P, Gleizes G, Barbey P (2009a) Decoupling between the middle and upper crust during transpression-related lateral flow: Variscan evolution of the Aston gneiss dome (Pyrenees, France). Tectonophysics 477(3–4):244–261

Denèle Y, Barbey P, Deloule E, Pelleter E, Olivier P, Gleizes G (2009b) Middle Ordovician U/Pb age of the Aston and Hospitalet orthogneissic laccoliths: their role in the Variscan evolution of the Pyrenees. Bull Soc Geol Fr 180(3):209–216

Denèle Y, Paquette JL, Olivier P, Barbey P (2011) Permian granites in the Pyrenees: the Aya pluton (Basque Country). Terra Nova 24(2):105–113

Denèle Y, Laumonier B, Paquette JL, Olivier P, Gleizes G, Barbey P (2014) Timing of granite emplacement, crustal flow and gneiss dome formation in the Variscan segment of the Pyrenees. Geol Soc London 405:265–287

Déramond J (1970) Tectoniques superposées dans le Paléozoïque du Haut-Salat (Pyrénées Ariégeoises), Thèse de 3ème cycle, Univ. Toulouse, France

Derré C (1973) Relations chronologiques entre la mise en place du granite de Salau (Haute Vallée du Salat, Pyrénées ariégeoises) et les déformations du Paléozoïque de la région. C R Acad Sci Paris 277:1279–1281

Derré C (1979) Le gisement de scheelite de Salau (Ariège, France). Chronique de la recherche minière 450:19–27

Derré C, Fonteilles M, Nansot YL (1980) Le gisement de scheelite de Salau, (Ariège, Pyrénées). 26ème CGI Gisements français, Paris. Fasc E9, 42 p

Derré C (1983) La province à Sn-W Ouest européenne. Histoire de divers types de gisements du massif Central, des Pyrénées et du Portugal. Distribution des gisements. Thèse de Doctorat d'état, Université Pierre et Marie Curie, Paris

Derré C, Lafitte M, Maury R (1984) Etude des minéralisations sulfurées du gisement de Salau, Pyrénées (France) et de ses environs. Mineral Deposita 19:176–182

Eichhorn R, Höll R, Loth G, Kennedy A (1999) Implications of U–Pb SHRIMP zircon data on the age and evolution of the Felbertal tungsten deposit (Tauern Window, Austria). Int J Earth Sci 88(3):496–512

Eldursi K, Branquet Y, Guillou-Frottier L, Marcoux E (2009) Numerical investigation of transient hydrothermal processes around intrusions: heat-transfer and fluid-circulation controlled mineralization patterns. Earth Planet Sci Lett 288:70–83

Fayek M, Kyser TK, Riciputi LR (2002) U and Pb isotope analysis of uranium minerals by ion microprobe and the geochronology of the McArthur River and Sue Zone uranium deposits, Saskatchewan, Canada. Can Mineral 40:1553–1569

Fonteilles M, Nansot L, Soler P, Zahm A (1988) Ore controls for the Salau Scheelite deposit (Ariège, France): evolution of ideas and present state of knowledge. Soc Geology Appl Mineral Deposits Spec Pub 6:95–116

Fonteilles M, Soler P, Demange M, Derré C, Krier-Schellen AD, Verkaeren J, Guy B, Zahm A (1989) The scheelite skarn deposit of Salau (Ariège, French Pyrenees). Econ Geol 84:1172–1209

Fosso Tchunte PM, Tchameni R, Andre-Mayer AS, Dakoure HS, Turlin F, Poujol M, Negue Nomo E, Saha Fouotsa AN, Rouer O (2018) Evidence for Nb-Ta occurrences in the syn-tectonic Pan-African Mayo Salah leucogranite (Northern Cameroon): constraints from Nb-Ta oxide mineralogy, geochemistry and U–Pb LA-ICP-MS geochronology on columbite and monazite. Minerals 8(5):188. https://doi.org/10.3390/min8050188

Frei R, Nägler TF, Schönberg R, Kramers JD (1998) Re-Os, Sm-Nd, U/Pb, and stepwise lead leaching isotope systematics in shear-zone hosted gold mineralization: genetic tracing and age constraints of crustal hydrothermal activity. Geochim Cosmochim Acta 62:1925–1936

Garcia-Sansegundo J, Poblet J, Alonso JL, Clariana P (2011) Hinterland-foreland zonation of the Variscan orogen in the Central Pyrenees: comparison with the northern part of the Iberian Variscan Massif. J Geol Soc London Spec Publ 349(1):169–184. https://doi.org/10.1144/SP349.9

Ghaderi M, Palin JM, Campbell IH, Sylvester PJ (1999) Rare earth element systematics in scheelite from hydrothermal gold deposits in the Kalgoorlie-Norseman region, Western Australia. Econ Geol 94:423–437

Guiraudie C, Prouhet JP, Passaqui B, Lorang M (1960) Campagne de prospection en 1960 sur les calcaires du Caradoc de l'Ariège. Rapport BRGM BRGG-A1760

Guiraudie C, Passaqui B, Prouhet JP (1963) Le gisement de Salau (Ariège), résultats généraux de la recherche au 01/11/1963. Rapport BRGM 63-DRMM-A-011

Gulson BL, Jones MT (1992) Cassiterite: potential for direct dating of mineral deposits and a precise age for the Bushveld complex granites. Geology 20:355–358

Guy B (1988) Contribution à l'étude des skarns de Costabonne (Pyrénées Orientales, France) et la théorie de la zonation métasomatique. Thèse de doctorat d'état de l'Université Pierre et Marie Curie, Paris

Harlaux M, Romer RL, Mercadier J, Morlot C, Marignac C, Cuney M (2018) 40 Ma of hydrothermal W mineralization during the Variscan orogenic evolution of the French Massif Central revealed by U/Pb dating of wolframite. Mineral Deposita 53(1):21–51

Harley SL, Kelly NM, Möller A (2007) Zircon behavior and the thermal histories of mountain chains. Elements 3:25–30

Horstwood MSA, Košler J, Gehrels G, Jackson SE, McLean NM, Paton C, Pearson NJ, Sircombe K, Sylvester P, Vermeesch P, Bowring JF, Condon DJ, Schoene B (2016) Community-derived standards for LA-ICP-MS U-(Th-)Pb geochronology – uncertainty propagation, age interpretation and data reporting. Geostand Geoanal Res 40:311–332

Jackson SE, Pearson NJ, Griffin WL, Belousova EA (2004) The application of laser ablation-inductively coupled plasma-mass spectrometry to in situ U–Pb zircon geochronology. Chem Geol 211:47–69

Kaelin JL (1982) Analyse structurale du gisement de scheelite de Salau (Ariège, France). Thèse doct. Ing. ENSMP, Paris

Krier-Schellen AD (1988) Etude microthermométrique des inclusions fluides des différentes paragenèses du gisement de scheelite (tungstène) de Salau (Pyrénées Ariégeoises, France). Thèse de l'Université Catholique de Louvain – La Neuve

Lang B, Edelstein O, Steinitz G, Kovacs M, Halga S (1994) Ar-Ar dating of adularia; a tool in understanding genetic relations between volcanism and mineralization; Baia Mare area (Gutii Mountains), northwestern Romania. Econ Geol Bull Soc Econ Geol 89(1):174–180

Laumonier B, Marignac C, Kister P (2010) Polymétamorphisme et évolution crustale dans les Pyrénées orientales pendant l'orogenèse varisque au Carbonifère supérieur. Bull Soc Géol Fr 181(5):411–428

Lecouffe J (1987) Les épisodes de fracturation dans le gisement de scheelite de Salau (Ariège), Caractères géométriques et pétrologiques, relation avec la minéralisation et implications minières. Thèse doct. Ing. ENSMP, Paris

Ledru P, Autran A (1987) Relationships between fluid circulation, ore deposition and shear zones: new evidence from the Salau scheelite deposit. Econ Geol 82:224–229

Lefebvre MG, Romer RL, Glodny J, Kroner U, Roscher M (2018) The Hämmerlein skarn-hosted polymetallic deposit and the Eibenstock granite associated greisen, western Erzgebirge, Germany: two phases of mineralization - two Sn sources. Mineral Deposita 126:1–22. https://doi.org/10.1007/s00126-018-0830-4

Lottermoser BG (1992) Rare earth elements and hydrothermal ore formation processes. Ore Geol Rev 7(1):25–41

Ludwig KR (2012) User's manual for a geochronological toolkit for Microsoft Excel. Berkeley Geochronol Cent 75

Ludwig KR, Grauch RI, Nutt CJ, Nash JT, Frishman D, Simmons KR (1987) Age of uranium mineralization at the Jabiluka and Ranger uranium deposits, Northern Territory, Australia: new U–Pb isotope evidence. Econ Geol 82:857–874

Mao M, Rukhlov AS, Rowins SM, Spence J, Coogan LA (2016) Apatite trace element compositions: a robust new tool for mineral exploration. Econ Geol 111:1187–1222

Marcoux E, Moëlo Y (1991) Lead isotope geochemistry and paragenetic study of inheritance phenomena in metallogenesis: examples from base metal sulfide deposits in France. Econ Geol 86:106–120

McDonough WF, Sun SS (1995) The composition of the Earth. Chem Geol 120(3–4):223–253

Melleton J, Gloaguen E, Frei D (2015) Rare-elements (Li-Be-Ta-Sn-Nb) magmatism in the European Variscan Belt, a review. In Proceedings of the 13th Biennial SGA Meeting, 24–27 August 2015, Nancy, France (eds. André-Mayer AS, Cathelineau M, Muchez P, Pirard E, Sindern S) 2:807–810

Morelli RM, Creaser RA, Selby D, Kontak DJ, Horne RJ (2005) Rhenium-osmium geochronology of arsenopyrite in Meguma group gold deposits, Meguma Terrane, Nova Scotia, Canada: evidence for multiple gold-mineralizing events. Econ Geol 100:1229–1242

Nabelek PI, Hofmeister AM, Whittington AG (2012) The influence of temperature-dependant thermal diffusivity on the conductive

cooling rates of plutons and temperature-time paths in contact aureoles. Earth Planet Sci Lett 317–318:157–164

Nakai S, Halliday AN, Kesler SE, Jones HD, Kyle JR, Lane TE (1993) Rb-Sr dating of sphalerites from Mississippi Valley-type (MVT) ore deposits. Geochim Cosmochim Acta 57:417–427

Ntiharirizwa S, Boulvais P, Poujol M, Branquet Y, Morelli C, Ntungwanayo J, Midende G (2018) Geology and U-Th-Pb dating of the Gakara REE Deposit, Burundi. Minerals 8(9):394. https://doi.org/10.3390/min8090394

Oze C, Cattell H, Grove M (2017) ^{40}Ar/ ^{39}Ar dating and thermal modeling of adularia to constrain the timing of hydrothermal activity in magmatic settings. Geology 45(1):43–46

Palau i Ramirez J (1998) El magmatisme calcoalcali del massis de Marimanya i les mineralitzacions As-Au-W associades. Institut Cartogràphic de Catalunya, Monografies tècniques 4

Palau i Ramirez J, Arcos D, Delgado J, Soler A (1995) Gold-bearing metasomatic bodies related to the Hercynian plutonism in the Marimanya area (Central Pyrenees, Spain). In Mineral deposits: From their origin to their environmental impacts 493–496

Palau i Ramirez J, Soler A, Solé J, Espinola MR, Delgado J (1997) Dating of gold-bearing skarns and intragranitic mineralizations in the Central Pyrenees. A new approach to thematic mapping. Second Congress on Regional Geological cartography and information systems, pp 53–58

Paquette JL, Piro JL, Devidal JL, Bosse V, Didier A, Sanac S, Abdelnour Y (2014) Sensitivity enhancement in LA-ICP-MS by N2 addition to carrier gas: application to radiometric dating of U-Th-bearing minerals. Agilent ICP-MS J 58:1–5

Petford N, Cruden AR, McCaffrey KJW, Vigneresse JL (2000) Granite magma formation, transport and emplacement in the Earth's crust. Nature 408:669–673

Pochon A, Poujol M, Gloaguen E, Branquet Y, Cagnard F, Gumiaux C, Gapais D (2016) U/Pb LA-ICP-MS dating of apatite in mafic rocks: evidence for a major magmatic event at the Devonian-Carboniferous boundary in the Armorican Massif (France). Am Mineral 101:2430–2442

Poulin RS, Kontak DJ, McDonald A, McClenaghan MB (2018) Assessing scheelite as an ore-deposit discriminator using its trace element and REE chemistry. Can Mineral 56(3):265–302

Raimbault L, Kaelin JL (1987) Pétrographie et géochimie de la granodiortite de la Fourque (gisement de scheelite de Salau, Pyrénées, France). Bull.Mineral. 110(6):633–644

Raimbault L, Baumer A, Dubru M, Benkerrou C, Croze V, Zahm A (1993) REE fractionation between scheelite and apatite in hydrothermal conditions. Am Mineral 78:1275–1285

Raju PVS, Hart CJR, Sangurmath P (2015) Scheelite geochemical signatures by LA-ICP-MS and potential for rare earth elements from Hutti Gold Mines and fingerprinting ore deposits. J Afr Earth Sci 114:220–227

Reyx J (1973) Relations entre tectonique, métamorphisme de contact et concentrations métalliques dans le secteur des anciennes mines d'Arre et d'Anglas (Hautes Pyrénées – Pyrénées atlantiques). Thèse doct. Ing. ENSMP, Paris

Romer RL, Lehmann B (1995) U/Pb columbite age of Neoproterozoic Ta-Nb mineralization in Burundi. Econ Geol 90:2303–2309

Romer RL, Lüders V (2006) Direct dating of hydrothermal W mineralization: U/Pb age for hübnerite ($MnWO_4$), Sweet Home Mine, Colorado. Geochim Cosmochim Acta 70:4725–4733

Romer RL, Soler A (1995) U-Pb age and lead isotope characterization of Au-bearing skarn related to Andorra granite (Pyrenees, Spain). Mineral Deposita 30:374–383

Romer RL, Wright JE (1992) U/Pb dating of columbites: a geochronological tool to date magmatism and ore deposits. Geochim Cosmochim Acta 56:2137–2142

Ruffet G, Innocent C, Michard A, Féraud G, Beauvais A, Nahon D, Hamelin B (1996) A geochronological ^{40}Ar/^{39}Ar and ^{87}Rb/^{86}Sr study of K–Mn oxides from the weathering sequence of Azul, Brazil. Geochim Cosmochim Acta 60:2219–2232

Sanematsu K, Watanabe K, Duncan RA, Izawa E (2006) The history of vein formation determined by ^{40}Ar/^{39}Ar dating of adularia in the Hosen-1 vein at the Hishikari epithermal gold deposit, Japan. Econ Geol Bull Soc Econ Geol 101(3):685–698

Smith SR, Foster GL, Romer RL, Tindle AG, Kelley SP, Noble SR, Horstwood M, Breaks FW (2004) U–Pb columbite–tantalite chronology of rare-element pegmatites using TIMS and laser ablation–multi collector–ICP–MS. Contrib Mineral Petrol 147:549–564

Smith SR, Kelley SP, Tindle AG, Breaks FW (2005) Compositional controls on ^{40}Ar/^{39}Ar ages of zoned mica from a rare-element pegmatite. Contrib Mineral Petrol 149(5):613–626

Soler P (1977) Pétrographie, thermochimie et métallogénie du gisement de scheelite de Salau (Pyrénées ariègeoises, France). Thèse doct. Ing. ENSMP, Paris

Soler A, Ayora C, Cardellach E, Delgado J (1990) Gold-bearing hédenbergite skarnsfrom the SW contact of the Andorra granite (central Pyrenees, Spain). Mineral Deposita 25:59–68

Song G, Qin K, Li G, Evans NJ, Chen L (2014) Scheelite elemental and isotopic signatures: implications for the genesis of skarn-type W-Mo deposits in the Chizhou Area, Anhui Province, Eastern China. Am Mineral 99(2–3):303–317

Spier CA, Vasconcelos PM, Oliveira SMB (2006) ^{40}Ar/^{39}Ar geochronological contraints on the evolution of lateritic iron deposits in the Quadrilatero Ferrifero, Minas Gerais, Brazil. Chem Geol 234:79–104

Stein HJ, Sundblad K, Markey RJ, Motuza G (1998) Re–Os ages for Archean molybdenite and pyrite, Kuittila-Kivisuo, Finland, and Proterozoic molybdenite, Kabeliai, Lithuania: testing the chronometer in a metamorphic and metasomatic setting. Mineral Deposita 33:329–345

Stein HJ, Morgan JW, Scherstén A (2000) Re-Os dating of low-level highly radiogenic (LLHR) sulfides: the Harnäs gold deposit, southwest Sweden, records continental-scale tectonic events. Econ Geol 95:1657–1671

Sylvester PJ, Ghaderi M (1997) Trace element analysis of scheelite by excimer laser ablation-inductively coupled plasma-mass spectrometry (ELA-ICPMS) using a synthetic silicate glass standard. Chem Geol 141:49–65

Timon Sanchez SM, Moro Benito MC, Cembranos Pérez ML (2009) Mineralogical and physiochemical evolution of the Los Santos scheelite skarn, Salamanca, NW Spain. Econ Geol 104:961–965

Toulhoat P (1982) Pétrographie et géochimie des isotopes stables (D/H, ^{18}O/^{16}O, ^{13}C/^{12}C, ^{34}S/^{32}S) des skarns du Quérigut. Comparaison avec les skarns à scheelite des Pyrénées. Thèse d'Université Paris VI

Van Achterbergh E, Ryan CG, Jackson SE, Griffin WL (2001) Data reduction software for LA-ICP-MS: appendix. In: Sylvester PJ (ed) Laser ablation-ICP mass spectrometry in the earth sciences: principles and applications. Mineralogical Association of Canada, Ottawa, pp 239–243

Vasconcelos PM, Becker TA, Renne PR, Brimhall GH (1992) Age and duration of weathering by ^{40}K–^{40}Ar and ^{40}Ar/^{39}Ar analysis of potassium-manganese oxides. Science 258:451–455

Vilà M, Pin C, Liesa M, Enrique P (2007) LPHT metamorphism in a late orogenic transpressional setting, Albera Massif, NE Iberia: implications for the geodynamic evolution of the Variscan Pyrenees. J Metamorph Geol 25(3):321–347. https://doi.org/10.1111/j.1525-1314.2007.00698.x

Vissers RLM, Meijer PT (2012) Iberian plate kinematics and Alpine collision in the Pyrenees. Earth-Sci Rev 114:61–83. https://doi.org/10.1016/j.earscirev.2012.05.001

Wintzer NE, Gillerman VS, Schmitz MD (2016) Eocene U/Pb scheelite LA-ICP-MS dates of stibnite-scheelite mineralization in the Yellow pine Au-Sb-W mining area, Central Idaho, USA. GSA annual meeting, Denver

Worrall F, Pearson D (2001) The development of acidic groundwaters in coal-bearing strata; part I, rare earth element fingerprinting. Appl Geochem 16(13):1465–1480

Yuan SD, Peng JT, Hu RZ, Li HM, Shen NP, Zhang DL (2008) A precise U–Pb age on cassiterite from the Xianghualing tin–polymetallic deposit (Hunan, South China). Mineral Deposita 43:375–382

Zhang YX, Liu YM, Gao SD, He QG (1990) Earth elements geochemical characteristics of tungstenic minerals: a distinguishing sign for ore-forming type. Geochimica 19:11–20